AD-A048 476 MCGILL UNIV MONTREAL (QUEBEC) F/G 4/2
A COMPARATIVE STUDY OF FRICTION AND NUMERICAL SMOOTHING IN A GL--ETC(U)
AUG 77 M M IBRAHIM F19628-77-C-0056
UNCLASSIFIED AFGL-TR-77-0177 NL

1 OF 1
ADA048476

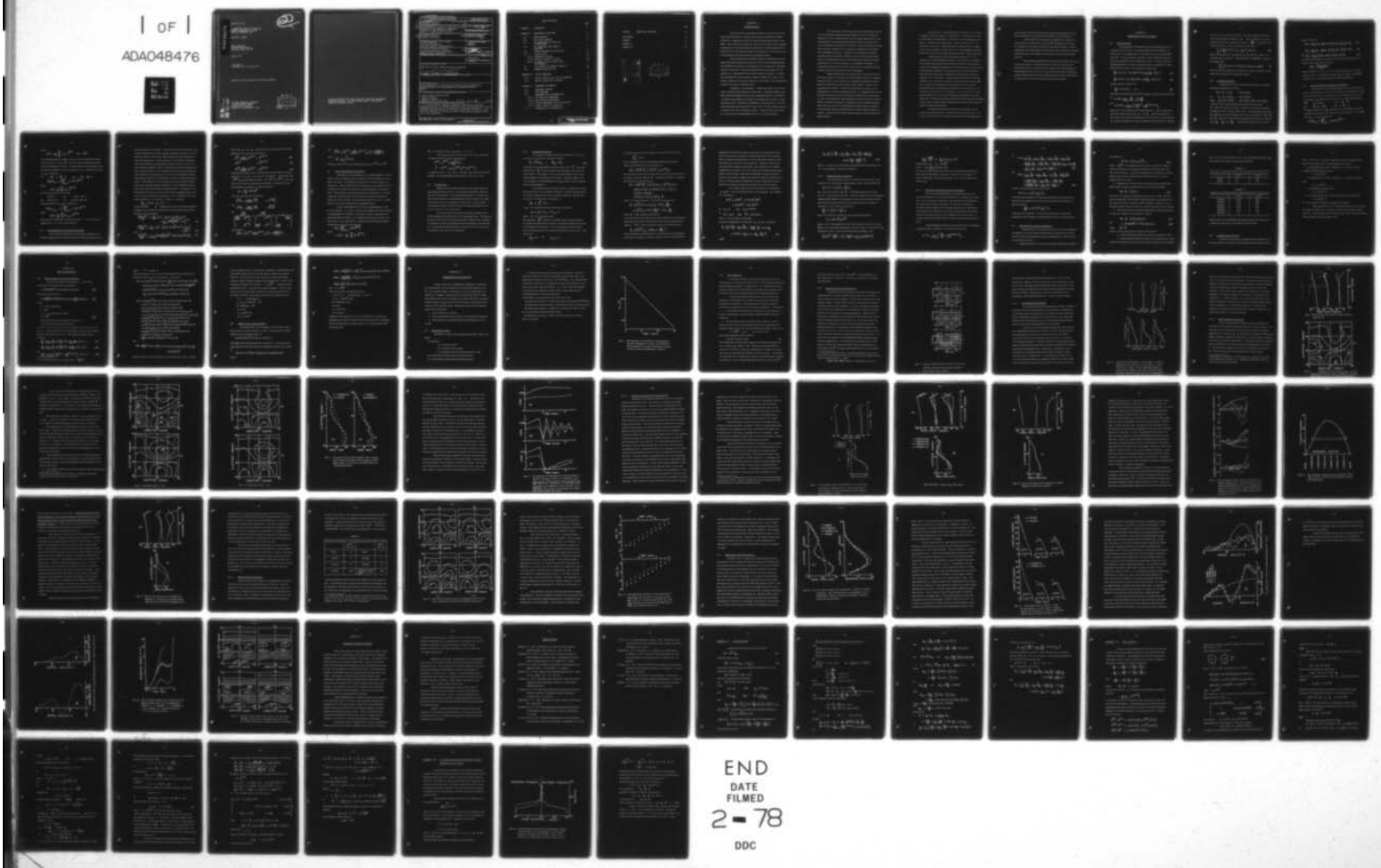

END
DATE FILMED
2-78
DDC

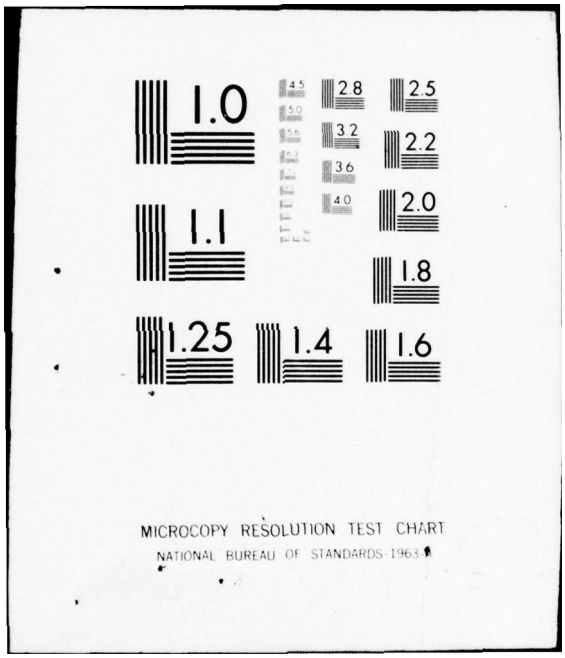
1.0
1.1
1.25
1.4
1.6
1.8
2.0
2.2
2.5
2.8
3.2
3.6
4.0
4.5
5.0
5.6
6.3
MICROCOPY RESOLUTION TEST CHART
NATIONAL BUREAU OF STANDARDS-1963

AFGL-TR-77-0177

A COMPARATIVE STUDY OF FRICTION AND NUMERICAL SMOOTHING IN A GLOBAL MODEL OF ATMOSPHERIC FLOW

Mostafa M. Ibrahim

McGill University
805 Sherbrooke Street W.
Montreal, Canada H3A 2K6

August, 1977

Final Report
1 November 1976 to 31 August 1977

AIR FORCE GEOPHYSICS LABORATORY
AIR FORCE SYSTEMS COMMAND
UNITED STATES AIR FORCE
HANSCOM AFB, MASSACHUSETTS 01731

Unclassified

SECURITY CLASSIFICATION OF THIS PAGE (When Data Entered)

(19) REPORT DOCUMENTATION PAGE	READ INSTRUCTIONS BEFORE COMPLETING FORM
(18) 1. REPORT NUMBER: AFGL-TR-77-0177 ✓	2. GOVT ACCESSION NO. / 3. RECIPIENT'S CATALOG NUMBER
(6) 4. TITLE (and Subtitle): A COMPARATIVE STUDY OF FRICTION AND NUMERICAL SMOOTHING IN A GLOBAL MODEL OF ATMOSPHERIC FLOW.	(9) 5. TYPE OF REPORT & PERIOD COVERED: Final Report. 1 Nov 76 - 31 Aug 77 / 6. PERFORMING ORG. REPORT NUMBER
(10) 7. AUTHOR(s): Mostafa M./Ibrahim	(15) 8. CONTRACT OR GRANT NUMBER(s): F19628-77-C-0056 new
9. PERFORMING ORGANIZATION NAME AND ADDRESS: McGill University, P.O. Box 6070, Station A, Montreal, Quebec, Canada H3C 3G1 ✓	10. PROGRAM ELEMENT, PROJECT, TASK AREA & WORK UNIT NUMBERS: 61102F, 2310G203
11. CONTROLLING OFFICE NAME AND ADDRESS: Air Force Geophysics Laboratory, Hanscom AFB, Massachusetts 01731 ✓, Monitor/Samuel Yee/LYD	(11) 12. REPORT DATE: Aug [redacted] 77 / 13. NUMBER OF PAGES: 88 (12) 88 p.
14. MONITORING AGENCY NAME & ADDRESS (if different from Controlling Office)	15. SECURITY CLASS. (of this report): Unclassified / 15a. DECLASSIFICATION/DOWNGRADING SCHEDULE

16. DISTRIBUTION STATEMENT (of this Report)

Approved for public release; distribution unlimited.

(16) 2310 / (17) G2

17. DISTRIBUTION STATEMENT (of the abstract entered in Block 20, if different from Report)

18. SUPPLEMENTARY NOTES

A thesis submitted to the Faculty of Graduate Studies and Research in partial fulfilment of the requirements for a degree of Master of Science

19. KEY WORDS (Continue on reverse side if necessary and identify by block number)

Global Primitive Equation Model
Linear viscosity
Numerical filtering
Numerical Stability Technique

223 150 GUL

20. ABSTRACT (Continue on reverse side if necessary and identify by block number)

A study is made of different techniques of assuring the long term numerical stability of a one-layer global primitive equation model which uses the pseudospectral technique for the evaluation of horizontal derivatives. It is found that numerical filtering is much more suitable than the use of a linear viscosity term both from the point of view of the stability achieved and the cost of the computation.

DD FORM 1 JAN 73 1473 EDITION OF 1 NOV 65 IS OBSOLETE

UNCLASSIFIED

SECURITY CLASSIFICATION OF THIS PAGE (When Data Entered)

TABLE OF CONTENTS

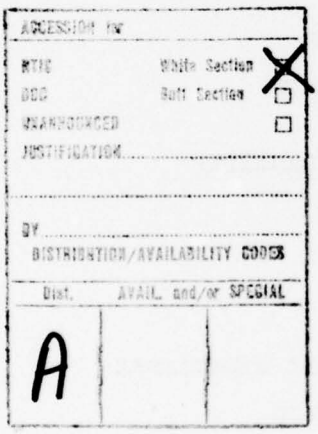

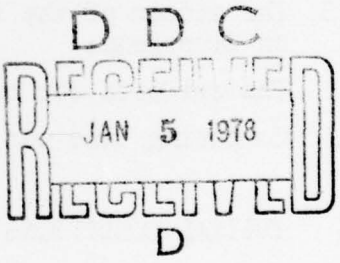

CHAPTER I

INTRODUCTION

There has been considerable concern in the past few years about the formulation of efficient and accurate numerical schemes suitable for integrating numerical weather prediction models on the globe. This interest has grown not only from the need to have weather predictions for the entire globe but also from the realization that for forecasts of more than a few days the introduction of artificial boundaries anywhere will deteriorate the forecast product.

The introduction of standard numerical techniques into the global prediction problem has proven to be far from straightforward. The difficulty is related to the singularity of the spherical coordinate system at the poles. The precise singularities at the poles can be avoided e.g. Merilees(1973) but a basic difficulty remains , namely , the convergence of the meridians requires excessively small time steps to ensure the numerical stability of the model. This requirement is costly in terms of computer time.

A second , more general , concern has been with the accuracy of numerical estimation of derivatives. Numerous studies have shown that the standard second order approximations to derivatives on standard gridlengths are simply not sufficiently accurate to make numerical error a secondary contributor to forecast error. For example Chouinard and Robert(1972) have shown that with 400km grid and a second order finite difference scheme , these errors may account for 20% of the rms geopotential error in a 36-hour forecast.

For both these reasons there has been considerable interest in the development of global spectral models in terms of spherical harmonics. Such a numerical basis has the double advantage of a lack of singularity in the numerical basis and no linear truncation error in the computation of derivatives. Further , by use of numerical rather than analytical transforms it is possible to implement such models with reasonable efficiency , certainly on 3rd generation computer systems presently available. However such a numerical basis does require a considerably amount of computation per degree of freedom and therefore it is wise to continue to investigate the viability of alternative schemes which are less costly than the complete spectral method yet have at least some of their advantages.

These consideration led Orszag(1972) to discuss the use of the linear property of the spectral method without going to a complete spectral model to get a method with considerable operational advantages over the spectral approximation. This method , known as the pseudospectral method , retains the traditional grid points for the representation of the meteorological fields , but expresses these fields as finite Fourier series for the purpose of estimation of derivatives. As such , the method can take advantage of the fast Fourier transform (FFT) to estimate derivatives. Orszag in the above mentioned paper shows that the error of the pseudospectral approximation compared to the spectral (Galerkin) approximation in some simple models are similar , despite the inclusion of aliasing terms in the pseudospectral approximation.

As mentioned , the pseudospectral algorithm is susceptible to apparent aliasing instability. This problem , which was first noted and discussed by Phillips(1959) , can lead to erroneous energy accumulation , specially in the short waves , and the " blow-up " of the calculation. We have to remember that this problem does not depend on the relation between the time increment and gridlength, and consequently is not removed by simply decreasing either of these quantities.

Merilees(1973 and 1974) developed an algorithm for the application of the pseudospectral method to the numerical integration of the shallow water equations and showed the ability of this scheme to solve time dependent problems and its superiority over the 4th-order finite difference schemes to reproduce accurate analytical solution given the same resolution. Jacques(1976) used the same methods to integrate a two-level model. In these studies the problem of aliasing instability was controlled by means of filtering where all wavelengths less or equal to 3-gridlengths are eliminated from time to time. Although using the 3-gridlength filter extends the calculation for 20 days without any indication of instability , it is a crude closure approximation because it is not a part of the governing equations. On the other hand , if the Fourier filter is performed every time step the model would be like a spectral model using Fourier series as basis functions instead of spherical harmonics.

Jacques(1976) noticed that the use of the periodic filter produced substantial errors , especially in low resolution runs. To remove this error and to control aliasing instability he suggested the

use of a filter which does not totally eliminate wavelengths less than three gridlengths or alternatively the addition of friction terms.

In this thesis we investigate the suggestion of Jacques by incorporating a viscous term in the momentum equations and also by studying in more detail the effect of periodic filtering. A further extension of the methodology results because the viscous term requires second derivative with respect to space which previous applications have not.

Even though Jacques(1976) was concerned with the simulation of baroclinic waves , the present work is entirely concerned with barotropic motion as represented by a shallow layer of homogeneous incompressible fluid. It will be seen that there are many interesting results which accrue from these experiments which are quite difficult to understand in spite the barotropic nature of the model.

CHAPTER II

DESCRIPTION OF THE MODEL

II.1 Basic equations

The equations of the model are those describing the flow of a shallow layer of water on a rotating sphere with the addition of a viscous force. One might think of this viscous force as an eddy diffusion term , but our purpose is simply to remove kinetic energy from the system, especially from small scale waves , in order to control aliasing instability. In terms of spherical polar coordinates (λ longitude and φ latitude) the momentum equations are

$$\frac{\partial u}{\partial t} + \mathbf{V}\cdot\nabla u - \left(f + \frac{u}{a}\tan\varphi\right)v + \frac{g}{a\cos\varphi}\frac{\partial h}{\partial \lambda} + \varepsilon F_\lambda = 0 , \qquad (1)$$

$$\frac{\partial v}{\partial t} + \mathbf{V}\cdot\nabla v + \left(f + \frac{u}{a}\tan\varphi\right)u + \frac{g}{a}\frac{\partial h}{\partial \varphi} + \varepsilon F_\varphi = 0 . \qquad (2)$$

And the continuity equation is

$$\frac{\partial h}{\partial t} + \nabla\cdot(h\mathbf{V}) = 0 . \qquad (3)$$

The advection and divergence terms are given in spherical coordinates as

$$\mathbf{V}\cdot\nabla A = \frac{u}{a\cos\varphi}\frac{\partial A}{\partial \lambda} + \frac{v}{a}\frac{\partial A}{\partial \varphi} ,$$

and

$$\nabla\cdot(A\mathbf{V}) = \frac{1}{a\cos\varphi}\left[\frac{\partial (Au)}{\partial \lambda} + \frac{\partial (Av\cos\varphi)}{\partial \varphi}\right] ,$$

where $\mathbf{V}$ is the velocity vector with component u and v (east-west and north-south respectively). F_λ and F_φ are the components of the viscous force with the formula given in section II.6.1. The symbol ε takes the values one or zero to identify that the friction is included

or not; a is the radius of the earth. The other symbols have their usual meteorological meaning. With $\varepsilon = 0$ equations (1) to (3) conserve all powers of potential vorticity ($\frac{\zeta + f}{h}$), where ζ is the relative vorticity. Also it is possible to show that

$$\int_A \frac{1}{2} \frac{\partial}{\partial t} \left[h(u^2 + v^2) + gh^2 \right] dA = 0, \qquad (4)$$

where the integration is carried all over the earth's surface. dA represent an area element ($\delta A = \Delta X . \Delta Y = a^2 \cos\varphi \, \Delta\lambda \, \Delta\varphi$). Equation (4) implies that

$$\int_\varphi \int_\lambda \left[h(u^2 + v^2) + gh^2 \right] \cos\varphi \, d\varphi \, d\lambda = \text{Constant}. \qquad (5)$$

The first term of equation (5) represents the kinetic energy while the second term represents the potential energy.

II.2 Grid point equations

Equations (1) to (3) are solved numerically on a latitude-longitude grid defined as follows

$$\varphi_J = \varphi_o - J \Delta\varphi, \qquad 1 \leq J \leq N_J,$$

and $$\lambda_I = (I-1) \Delta\lambda, \qquad 1 \leq I \leq N_I,$$

where $\varphi_o = \pi/2 + \Delta\varphi/2$, $\Delta\varphi = \pi/N_J$ and $\Delta\lambda = 2\pi/N_I$,

$\Delta\varphi$ and $\Delta\lambda$ are latitudinal and longitudinal increments. This definition avoids grid points at the poles which are considered as singular points, as $\Delta\lambda$ goes to zero. The momentum and continuity equations are thus satisfied every where on the grid. If δ_t, δ_φ and δ_λ denote the finite difference operators which are to approximate $\frac{\partial}{\partial t}$, $\frac{\partial}{\partial \varphi}$ and $\frac{\partial}{\partial \lambda}$ respectively, then (1) to (3) can be

written in the form

$$\delta_t u = -\frac{u}{a\cos\varphi}\,\delta_\lambda u - \frac{v}{a}\delta_\varphi u + \left(f + \frac{u}{a}\tan\varphi\right)v - \frac{g}{a\cos\varphi}\,\delta_\lambda h - \varepsilon F_\lambda , \qquad (6)$$

$$\delta_t v = -\frac{u}{a\cos\varphi}\,\delta_\lambda v - \frac{v}{a}\delta_\varphi v - \left(f + \frac{u}{a}\tan\varphi\right)u - \frac{g}{a}\delta_\varphi h - \varepsilon F_\varphi , \qquad (7)$$

and

$$\delta_t h = -\frac{1}{a\cos\varphi}\left[h\,\delta_\lambda u + u\,\delta_\lambda h + \delta_\varphi\left(h v\cos\varphi\right)\right]. \qquad (8)$$

A centered finite difference scheme is used for the left hand side of the above three equations, as follow

$$\delta_t A = \frac{A_{t+\Delta t} - A_{t-\Delta t}}{2\Delta t} ,$$

where A stands for u, v or h. For the first time step, a forward scheme is used. For space derivatives δ_λ and δ_φ, a pseudospectral scheme is used as described in the following section.

II.3 The pseudospectral definition of derivatives

The definition of the pseudospectral derivatives as used is described by Merilees (1974), but for the sake of completness we shall review the definition. In spherical polar coordinates let us consider the variable $A_{n,m}$ defined at grid point (n, m), $A_{n,m} = A(\lambda_n, \varphi_m)$, where

$$\lambda_n = (n-1)\,\Delta\lambda \quad ; \quad 1 \leq n \leq 2N,$$

and

$$\varphi_m = \varphi_0 - m\,\Delta\varphi \quad ; \quad 1 \leq m \leq M.$$

The approximation for $\partial/\partial\lambda$ presents no special problem since the variables are periodic of λ and do not involve the pole. The lamda-derivative of $A_{n,m}$ is defined as

$$\left(\delta_\lambda A\right)_{n,m} = \sum_{k=-(N-1)}^{(N-1)} ik\,a_m(k)\,e^{ikn\Delta\lambda} ,$$

where

$$a_m(k) = \frac{1}{2N} \sum_{m=1}^{2N} A_{n,m}\, e^{-ikn\Delta\lambda} \quad \text{and} \quad i = \sqrt{-1}\ .$$

For the approximation of $\partial/\partial\varphi$, we have to be more careful since we cross the poles. In this case we have to know whether the variable is vector component or scalar. A scalar quantity is continuous at the pole while, in general, a vector component is not. The phi-derivative of $A_{n,m}$ is defined as

for $1 \leq m \leq M$ and $1 \leq n \leq N$,

$$(\delta_\varphi A)_{n,m} = \sum_{l=-(M-1)}^{(M-1)} il\, b(l)\, e^{ilm\Delta\varphi},$$

where

$$b(l) = \frac{1}{2M} \sum_{m=1}^{2M} A_{n,m}\, e^{-ilm\Delta\varphi}\ .$$

For grid point (LM, LN) such that

$LM = N+n$ for $1 \leq n \leq N$,

and $LN = 2M-m+1$ for $M+1 \leq m \leq 2M$,

the phi-derivative of $A_{LM,LN}$ is defined as

$$(\delta\varphi)_{LM,LN} = S \sum_{l=-(M-1)}^{(M-1)} il\, b(l)\, e^{ilm\Delta\varphi},$$

where

$$b(l) = \frac{-S}{2M} \sum_{m=1}^{2M} A_{LM,LN}\, e^{-ilm\Delta\varphi}\ .$$

In the previous definition of the phi-derivative $s=-1$ for a scalar quantity and $s=+1$ for a vector quantity.

II.4 One dimensional semi-implicit algorithm

The numerical integration of the dynamic equations on a latitude-longitude grids requires excessively small time steps due to

the convergence of meridians. Merilees et al (1976) show that the use of space filtering in the polar regions (generally used before to avoid this restriction) cause errors which lead to artificial transports of mass and momentum. In the same paper a semi-implicit technique with one-dimension is used instead of the polar filter. The use of a semi-implicit scheme in order to increase the time step makes sense from a physical point of view, because it modifies only the high frequency motions whereas the polar filter does not distinguish between low and high frequency waves leading to errors in the meteorological modes. The solution of the one-dimensional semi-implicit scheme makes use of the fast Fourier transform, so the replacement of the polar filter adds little additional computing time. In equations (1) to (3) the terms which give rise to gravity wave propagation along a latitude circle are treated semi-implicitly. This means that (2) will be treated explicitly. If we define a variable A such that

$$A^{\tau}_{I,J} = A(\lambda_I, \varphi_J, t_\tau)$$

where $t_\tau = \tau \Delta t$, Δt being the time step, the numerical approximation to the primitive equations (6) to (8) at grid point (I, J) and time t_τ can be written as

$$\frac{u^{\tau+\Delta t} - u^{\tau-\Delta t}}{2\Delta t} = -\frac{u^{\tau}}{a\cos\varphi}\delta_\lambda u^{\tau} - \frac{v}{a}\delta_\varphi u^{\tau} - \left(f + \frac{u^{\tau}}{a}\tan\varphi\right)v^{\tau} - \frac{g}{a\cos\varphi}\frac{\delta_\lambda h^{\tau+\Delta t} + \delta_\lambda h^{\tau-\Delta t}}{2} - \varepsilon F_\lambda^{\tau-\Delta t}, \qquad (9)$$

$$\frac{v^{\tau+\Delta t} - v^{\tau-\Delta t}}{2\Delta t} = -\frac{u^{\tau}}{a\cos\varphi}\delta_\lambda v^{\tau} - \frac{v^{\tau}}{a}\delta_\varphi v^{\tau} - \left(f + \frac{u^{\tau}}{a}\tan\varphi\right)u^{\tau} - \frac{g}{a}\delta_\varphi h^{\tau} - \varepsilon F_\varphi^{\tau-\Delta t}, \qquad (10)$$

and

$$\frac{h^{\tau+\Delta t} - h^{\tau-\Delta t}}{2\Delta t} = -\frac{1}{a\cos\varphi}\left[\bar{H}^{\tau}\frac{(\delta_\lambda u^{\tau+\Delta t} + \delta_\lambda u^{\tau-\Delta t})}{2} + u^{\tau}\delta_\lambda h^{\tau} + \delta_\varphi(h^{\tau}v^{\tau}\cos\varphi)\right]. \qquad (11)$$

Notice that F_λ and F_φ in (9) and (10) are calculated at time $\tau-\Delta t$. Equations (9) to (11) can be written as

$$u^{\tau+\Delta t} + \frac{g\,\Delta t}{a\cos\varphi}\,\delta_\lambda h^{\tau+\Delta t} = U^{\tau,\tau-\Delta t} \tag{12}$$

$$v^{\tau+\Delta t} = V^{\tau,\tau-\Delta t} \tag{13}$$

$$h^{\tau+\Delta t} + \frac{\bar{H}^{\tau}\Delta t}{a\cos\varphi}\,\delta_\lambda u^{\tau+\Delta t} = H^{\tau,\tau-\Delta t} \tag{14}$$

The right hand side of (12), (13) and (14) can be calculated, they are function of u, v and h at times τ and $\tau-\Delta t$. This means that $v^{\tau+\Delta t}$ can be calculated from (13). For $u^{\tau+\Delta t}$ and $h^{\tau+\Delta t}$, let us consider (12) and (14) for a particular zonal mode k, using the Fourier representation a variable A can be written as

$$A = \sum_k A(k)\, e^{ik\lambda}$$

Then (12) and (14) can be written as

$$u^{\tau+\Delta t}(k) + \frac{ikg\,\Delta t}{a\cos\varphi}\,h^{\tau+\Delta t}(k) = U^{\tau,\tau-\Delta t}(k),$$

and

$$h^{\tau+\Delta t}(k) + \frac{ik\bar{H}\,\Delta t}{a\cos\varphi}\,u^{\tau+\Delta t}(k) = H^{\tau,\tau-\Delta t}(k).$$

Or

$$\frac{u^{\tau+\Delta t}(k)}{\begin{vmatrix} \frac{ikg\Delta t}{a\cos\varphi} & -U^{\tau,\tau-\Delta t} \\ 1 & -h^{\tau,\tau-\Delta t} \end{vmatrix}} = \frac{-h^{\tau+\Delta t}(k)}{\begin{vmatrix} 1 & -U^{\tau,\tau-\Delta t} \\ \frac{ik\bar{H}^{\tau}\Delta t}{a\cos\varphi} & -h^{\tau,\tau-\Delta t} \end{vmatrix}} = \frac{1}{\begin{vmatrix} 1 & \frac{ikg\Delta t}{a\cos\varphi} \\ \frac{ik\bar{H}^{\tau}\Delta t}{a\cos\varphi} & 1 \end{vmatrix}},$$

which leads to

$$u^{\tau+\Delta t}(k) = \left[U^{\tau,\tau-\Delta t} - \frac{ikg\,\Delta t}{a\cos\varphi}\,H^{\tau,\tau-\Delta t}\right] \Big/ \left[1 + \frac{k^2 g\bar{H}^{\tau}(\Delta t)^2}{a^2\cos^2\varphi}\right],$$

and $$h^{\tau+\Delta t}(k) = \left[h^{\tau,\tau-\Delta t} - \frac{ik\bar{H}^{\tau}\Delta t}{a\cos\varphi} U^{\tau,\tau-\Delta t} \right] \Big/ \left[1 + \frac{k^2 g \bar{H}^{\tau}(\Delta t)^2}{a^2\cos^2\varphi} \right],$$

where $$\bar{H}^{\tau} = \frac{1}{2\pi} \int_0^{2\pi} h^{\tau}\, d\lambda \ .$$

Finally by inverse Fourier transformation we get $u^{\tau+\Delta t}$ and $h^{\tau+\Delta t}$.

II.5 Three gridlength and time filters

As stated in the introduction, it is usually necessary to have some sort of smoothing to ensure stability of the calculation for more than a few days. The instability is believed to be the so-called non-linear type. Orszag (1971) shows that aliasing can be eliminated if the variables are filtered with respect to three gridlength waves and smaller. This filtering, used each time step or periodically, for initial conditions corresponding to Haurwitz waves, keeps the integration stable for at least 20 days, the maximum period of our runs. In what follows we call this smoothing the 3-gridlength filter.

In the 3-gridlength filter, Fourier representation is used for the variables u, v and h then all wavelengths less than or equal to 3-gridlengths are filtered. This filter is done in both east-west and north-south directions. For example with N points around a latitude circle, if A_n represents a variable before filtering and A_n^* the variable after east-west filtering then

$$A_n^* = \sum_{k=-(K_m-1)}^{(K_m-1)} \alpha(k)\, e^{ikn\Delta\lambda},$$

where

$$\alpha(k) = \frac{1}{N} \sum_{n=1}^{N} A_n\, e^{-ikn\Delta\lambda},$$

k_m is the largest integer contained in $N/3 + 0.5$.

The model also makes use of a weak time filter developed by Robert (1966) by the following algorithm

$$F^{\tau+\Delta t} = F^{*\tau-\Delta t} + \left(\frac{\partial F}{\partial t}\right)^{\tau} 2\Delta t,$$

$$F^{\tau} = F^{*\tau} + \alpha\left[F^{\tau+\Delta t} - 2F^{\tau} + F^{*\tau-\Delta t}\right].$$

F stands for any of u, v and h. The (*) indicates a time filtered variable. In the experiments reported here α is set at 0.02.

II.6 Friction term

Because of the limited resolution of the models which predict geophysical fluid motion, it is generally impossible to describe the small scale motions. Through turbulence theory, it may be possible to describe their average behaviour and their effect on the large scale motion. One of the simplest of these ideas is that of energy cascading from large to small scales to be finally dissipated by molecular viscosity at very small scales.

As is clear from our previous discussion a friction term will be studied as an alternative to the 3-gridlength filter. The primary purpose of this term is to prevent non-linear instability and, hopefully, to represent in a more sophisticated way what happens in the atmosphere. In the following three sections a discussion of the viscous force as included in this work will be presented.

II.6.1 Mathematical formula

In a general coordinate system the definition of friction or viscous force is given by McConnell (1931) as

$$F_r = g^{st} \sigma_{rs,t} \quad ; \quad g^{st} g_{tr} = \delta^s_r \,, \tag{15}$$

where g_{st} is the fundamental or metric tensor, and g^{st} is its contravarient form, δ^s_r is the Kronecker delta and σ_{rs} is the viscosity stress tensor. The indices (r, s, t) in the tensor notation take values corresponding to the dimension of the space. Repeated indices are to be summed over the dimensions of the space and a comma indicates covarient differentiation.

For equation (15) to be useful we have to express the stress as function of the other variables of the flow. We know that the stress is function of strain and as usual we shall use Hooke's postulate that the stress is a linear function of strain, or

$$\sigma_{rs} = \gamma^{mn}_{rs} \, e_{mn} \,.$$

e_{mn} is actually the velocity strain tensor defined as

$$e_{mn} = \tfrac{1}{2} (V_{m,n} + V_{n,m}) \,,$$

where V_s is the velocity vector.

The quantities γ^{mn}_{rs} which form a mixed tensor of the forth order, are called the coefficients of viscosity. We shall assume that the fluid is homogeneous and isotropic. For a homogeneous fluid the same strain at different point of the medium produces the same stress. This means that

$$\sigma_{rs,t} = 0 \quad \text{if} \quad e_{rs,t} = 0 \,.$$

A necessary and sufficient condition for the above to hold is that

$$\gamma^{mn}_{rs,t} = 0 .$$

For an isotropic fluid the most general isotropic fourth order tensor with symmetry in (r, s) and (m, n) is

$$\gamma^{mn}_{rs} = \mu\left(\delta^m_r \delta^n_s + \delta^n_r \delta^m_s\right) + \lambda' g^{mn} g_{rs} .$$

The first term is known as the first viscosity and the second term as the second viscosity; μ and λ' are elastic constants. It follows that the stress can be written as

$$\begin{aligned}
\sigma_{rs} &= \mu\left(\delta^m_r \delta^n_s + \delta^n_r \delta^m_s\right) e_{mn} + \lambda' g^{mn} g_{rs} e_{mn} , \\
&= \mu\left(e_{rs} + e_{sr}\right) + \tfrac{1}{2}\lambda' g_{rs}\left(V^n_{.,n} + V^m_{.,m}\right) , \\
&= 2\mu e_{rs} + \lambda' g_{rs} D , \\
&= \mu\left(V_{r,s} + V_{s,r}\right) + \lambda' g_{rs} D ,
\end{aligned}$$

where D is the divergence. It follows that (15) becomes

$$\begin{aligned}
F_r &= \mu g^{st}\left(V_{r,s} + V_{s,r}\right)_{,t} + \lambda' g_{rs} \frac{\partial D}{\partial x^t} , \\
&= \mu\left\{g^{st} V_{r,st} + k V_r + \frac{\partial D}{\partial x^r}\right\} + \lambda' g_{rs} \frac{\partial D}{\partial x^t} ,
\end{aligned}$$

where k is the curvature of the earth.

It is clear that the last term does not add anything new to the equation and because we use the viscous force to get its smoothing effect we shall put $\lambda' = 0$. Thus the friction we have used takes the form

$$F_r = \mu\left\{g^{st} V_{r,st} + k V_r + \frac{\partial D}{\partial x^r}\right\} .$$

While the shallow water equations on a sphere have a time-honoured usefulness for studying numerical schemes and can be derived with

appropriate limiting assumptions, the form for a spherical friction force has not been so carefully treated especially as to its limiting form for quasi-horizontal flow. We have arbitrarily chosen to consider the flow to be strictly two dimensional. However it will be our contention that a simple friction term, with coefficient of viscosity independent of the flow, is not very useful for controlling aliasing instability for the simple reason that the Reynolds number required at the scale of the grid is simply too small not to affect the scales of interest. In other words the magnitude of friction required to control numerical instability excessively smooths the scales of interest.

For surface spherical polar coordinate in two dimension λ and φ ; φ is the latitude and λ is the longitude. The distance ds is defined as

$$(ds)^2 = a^2(d\varphi)^2 + a^2(\cos\varphi)^2(d\lambda)^2,$$

$$= g_{11}(dx_1)^2 + g_{22}(dx_2)^2 .$$

So $g_{11} = a^2$ and $g_{22} = a^2\cos^2 x_1$

or $g^{11} = 1/a^2$ and $g^{22} = 1/a^2\cos^2 x_1$,

where a is the radius of the earth.

As shown in appendix (I) we find that F_λ and F_φ are given by

$$F_\lambda = \frac{\nu}{a^2}\left\{ \frac{\partial^2 u}{\partial\varphi^2} + \frac{1}{\cos\varphi}\frac{\partial^2 v}{\partial\varphi\partial\lambda} - \frac{3\sin\varphi}{\cos^2\varphi}\frac{\partial v}{\partial\lambda} - \tan\varphi\frac{\partial u}{\partial\varphi} \right.$$

$$\left. - \left(2\tan^2\varphi - \frac{1}{\cos^2\varphi}\right)u + \frac{2}{\cos^2\varphi}\frac{\partial^2 u}{\partial\lambda^2} \right\}, \qquad (16)$$

and

$$F_\varphi = \frac{\nu}{a^2}\left\{2\frac{\partial^2 v}{\partial\varphi^2} + \frac{1}{\cos\varphi}\frac{\partial^2 u}{\partial\varphi\partial\lambda} + \frac{1}{\cos^2\varphi}\frac{\partial^2 v}{\partial\lambda^2} + \frac{3\sin\varphi}{\cos^2\varphi}\frac{\partial u}{\partial\lambda}\right.$$

$$\left. -2\tan\varphi\frac{\partial v}{\partial\varphi} - \frac{2\sin^2\varphi}{\cos^2\varphi}v\right\}, \qquad (17)$$

where u and v are the horizontal components of the wind vector and ν is the kinematic viscosity coefficient.

II.6.2 Analytical effect of friction

One of the useful features of the friction term used is that if the flow is (horizontally) non-divergent, then it can be shown that

$$\mathbf{k}\cdot\nabla\wedge\mathbf{F} = \nu\left[\nabla^2\zeta + \frac{2\zeta}{a^2}\right],$$

$\mathbf{k}$ is the unit vertical vector, $\mathbf{F}$ is the horizontal friction vector and ζ is the relative vorticity. Since the condition of non-divergence implies that the shallow water equations reduce to the vorticity equation, then using the previous formula and considering that the change in vorticity is due to friction we can write

$$\frac{\partial\zeta}{\partial t} = \nu\left[\nabla^2\zeta + \frac{2\zeta}{a^2}\right].$$

Now if we write the vorticity as a pure spherical harmonic

$$\zeta = A(t)\, P_n^m(\varphi)\, e^{im\lambda},$$

where $A(t)$ is the amplitude of the vorticity which is function of time, $P_n^m(\varphi)$ is the associated polynomial of the first kind, m is the east-west wavenumber and n is the two dimensional wavenumber, then

$$P_n^m(\varphi)\, e^{im\lambda}\frac{\partial A(t)}{\partial t} = \nu\left[-\frac{n(n+1)}{a^2} + \frac{2}{a^2}\right] A(t)\, P_n^m(\varphi)\, e^{im\lambda},$$

or

$$\frac{1}{A(t)} \frac{\partial A(t)}{\partial t} = -\frac{\nu}{a^2} \{ n(n+1) - 2 \}.$$

Integrating we get $A = A_0 e^{-\alpha t}$,

where $\alpha = \nu/a^2 \{ n(n+1) - 2 \}$.

So we can see that the effect of friction, is to reduce the amplitude of the vorticity exponentially with time. The effect will be larger for small wavelengths or large wavenumbers, as it is clear from the formula for α.

II.6.3 The effect of the friction term on divergence

The initial conditions used in our experiments are such that the divergence and its first time derivative is initially zero. However, due to non-linear interaction, even with the above initial condition significant divergence develops. The problem of aliasing is associated with the appearance of wiggles and increase of divergence. In this section it is desirable to show that the amplitude of the divergence field will decrease due to the existence of the friction term, or in other words the divergence field is as well controlled by the friction force.

Using equations (16) and (17) with the definition of divergence in spherical polar coordinate, it is possible to show that

$$\nabla . F = \frac{1}{a \cos\varphi} \left[\frac{\partial F_\lambda}{\partial \lambda} + \frac{\partial (F_\varphi \cos\varphi)}{\partial \varphi} \right],$$

or

$$\nabla . F = \frac{2}{a^3}\frac{\partial^3 v}{\partial \varphi^3} + \frac{2}{a^3\cos\varphi}\frac{\partial^3 u}{\partial \varphi^2 \partial \lambda} + \frac{2}{a^3\cos^2\varphi}\frac{\partial^3 v}{\partial \varphi \partial \lambda^2} + \frac{2}{a^3\cos^3\varphi}\frac{\partial^3 u}{\partial \lambda^3}$$
$$+ \frac{2\sin\varphi}{a^3\cos^2\varphi}\frac{\partial^2 u}{\partial \varphi \partial \lambda} - 4\frac{\sin\varphi}{a^3\cos\varphi}\frac{\partial^2 v}{\partial \varphi^2} - 2\frac{\sin\varphi}{a^3\cos^3\varphi}\frac{\partial^2 v}{\partial \lambda^2} + \frac{2}{a^3\cos\varphi}\left(1+\frac{1}{\cos\varphi}\right)\frac{\partial u}{\partial \lambda}$$
$$- \frac{2}{a^3\cos^2\varphi}\frac{\partial v}{\partial \varphi} - \frac{2}{a^3\cos\varphi}\left(\sin\varphi + \frac{\sin\varphi}{\cos^2\varphi}\right) v \,, \qquad (18)$$

and

$$\nabla^2 D = \frac{1}{a^3\cos^3\varphi}\frac{\partial^3 u}{\partial \lambda^3} + \frac{1}{a^3\cos^2\varphi}\frac{\partial^3 v}{\partial \varphi \partial \lambda^2} + \frac{1}{a^3}\frac{\partial^3 v}{\partial \varphi^3} - \frac{\sin\varphi}{a^3\cos^3\varphi}\frac{\partial^2 v}{\partial \lambda^2}$$
$$+ \frac{2\sin\varphi}{a^3\cos^2\varphi}\frac{\partial^2 u}{\partial \varphi \partial \lambda} + \frac{1}{a^3\cos\varphi}\frac{\partial^3 u}{\partial \varphi^2 \partial \lambda} - \frac{\sin\varphi}{a^3\cos\varphi}\frac{\partial^2 v}{\partial \varphi^2}$$
$$+ \left(\frac{\sin^2\varphi - 2}{a^3\cos^3\varphi}\right)\frac{\partial v}{\partial \varphi} + \frac{1}{a^3\cos^3\varphi}\frac{\partial u}{\partial \lambda} - \frac{\sin\varphi}{a^3\cos^3\varphi} v \,. \qquad (19)$$

So from (18) and (19) one can conclude that

$$\nabla . F = 2\left(\nabla^2 + \frac{1}{a^2}\right) D$$

If we take the divergence of the momentum equation and considering that the local change of the wind is governed only by the friction we get the formula

$$\frac{\partial D}{\partial t} = 2\nu\left(\nabla^2 + \frac{1}{a^2}\right) D$$

From the above equation, it is clear that the friction reduces the amplitude of the divergence except probably for the very large scales.

II.7 The criteria for numerical stability

The guidelines for the choice of time step for the integration of equations (1) to (3) have been determined by an analysis of the CFL criteria in Cartesian geometry as given in appendix II. These criteria are summarized below.

1. Neglecting the friction terms and using a fully explicit scheme,

the condition is

$$\Delta t \leq 1/(L^2+k^2)^{\frac{1}{2}}c, \tag{20}$$

where $c=(g\bar{H})^{\frac{1}{2}}$ is the speed of gravity waves; L and K are respectively the maximum wavenumbers permitted in the north-south and east-west directions. As shown in appendix II the inclusion of friction terms in fully explicit scheme does not affect the CFL criterion significantly in our case.

2. Neglecting the friction terms and using the one dimensional semi-implicit scheme as described in II.4 the condition reads

$$\Delta t \leq 1/Lc. \tag{21}$$

Due to the convergence of meridians near the poles $K \gg L$ and thus the one dimensional semi-implicit algorithm permit much longer time step than those given by the fully explicit scheme. However, if two dimensional semi-implicit scheme is used all the modes will be neutral.

3. With friction and the one dimensional semi-implicit algorithm we have two conditions to be satisfied, they are

$$\Delta t \leq 1/2\nu(K^2+L^2), \tag{22}$$

and

$$1 \geq \Phi(\Delta t)^2L^2 + \nu(\Delta t)(K^2+L^2), \tag{23}$$

where $\Phi = g\bar{H}$.

In fact, we can summarize the result of this case as

a. If ν is relatively small the condition for stability is (21).

b. As ν becomes larger the condition for stability goes to (22).

To show the difference between the time steps as given by the conditions

(20), (21), (22) and (23) tables 1 and 2 give the approximate time step, in seconds, from the above mentioned criterions.

TABLE 1.

Experiment notation	Δt from condition (20) (sec)	Δt from condition (21) (sec)
N3216	143	1785
N6432	35	892

TABLE 2.

Experiment notation	Δt from condition (22) (sec)	Δt from condition (23) (sec)
F3216(4)	8×10^4	1785
F3216(5)	8×10^3	1785
F3216(6)	8×10^2	800
F6432(4)	5×10^3	892
F6432(5)	5×10^2	500
F6432(6)	50	50

Experiments with 3-gridlength filter applied each time step permit a longer time step due to the removal of short waves.

II.8 Computing time per step

A CDC 7600 computer in single precision arithmetic (60 bit word length) was used for all the experiments discussed in this

thesis. The time, in seconds, required per step of integration for the one level model used are approximately as follows:

a. Including Fourier filter, applied to u, v and h, for two successive steps each three hours

$$T = 0.22 \times 10^{-3} \; D.$$

b. Including Fourier filter, applied to u, v and h, each time step

$$T = 0.27 \times 10^{-3} \; D.$$

c. Including the viscous force

$$T = 0.32 \times 10^{-3} \; D.$$

d. Including neither the viscous force nor the Fourier filter

$$T = 0.21 \times 10^{-3} \; D.$$

D is the number of degrees of freedom of the model.

This means that the use of the periodic filter (two successive steps per three hours) increases the time of calculation by less than 5% ; filtering each time step by less than 29% ; while the viscous force increases the time by about 52%.

CHAPTER III

INITIAL CONDITIONS

III.1 Initial condition for the test experiment

The field is initially non divergent or u and v are calculated from a stream function defined as

$$\psi = a^2 k_1 (\cos\varphi)^m \sin\varphi \cos(m\lambda - \omega t) - a^2 \Lambda \sin\varphi, \quad * \qquad (24)$$

The height field is given by

$$h = \frac{2\Omega a^2 k_2}{g} (\cos\varphi)^m (\sin\varphi)^2 \cos(m\lambda - \omega t) + \frac{\Omega \Lambda a^2}{g} (\cos\varphi)^2 + h_0, \qquad (25)$$

where

m is the wavenumber,

t time,

k, k_2, Λ, ω and h_0 are constant,

$$k_1 = k\, e^{-\alpha t}, \qquad (26)$$

α is function of the wavenumber (see II.6.2),

Ω is the angular velocity of the earth.

u, v and h given by (24) and (25) do not generally satisfy (1) to (3). To make u, v and h satisfy (1) to (3) for all times, an extra term is added to each of the equations (1) to (3). The modified equations can be written as

$$\frac{\partial u}{\partial t} + \frac{u}{a\cos\varphi}\frac{\partial u}{\partial \lambda} + \frac{v}{a}\frac{\partial u}{\partial \varphi} - f^* v + \frac{g}{a\cos\varphi}\frac{\partial h}{\partial \lambda} - F_\lambda - G u = 0, \qquad (27)$$

$$\frac{\partial v}{\partial t} + \frac{u}{a\cos\varphi}\frac{\partial v}{\partial \lambda} + \frac{v}{a}\frac{\partial v}{\partial \varphi} + f^* u + \frac{g}{a}\frac{\partial h}{\partial \varphi} - F_\varphi - G v = 0, \qquad (28)$$

and

$$\frac{\partial h}{\partial t} + \frac{1}{a\cos\varphi}\left[\frac{\partial (hu)}{\partial \lambda} + \frac{\partial (hv\cos\varphi)}{\partial \varphi}\right] - G h = 0, \qquad (29)$$

---

* i.e. the wave component is proportional to $P^m_{m+1}(\varphi)$.

where $f^* = f + u \tan\varphi / a$.

The expressions for Gu, Gv and Gh are obtained by substituting u, v and h from (24) and (25) in (27) and (29). This gives

$$G_u = \alpha m (\cos\varphi)^{m-1} (\sin\varphi)^2 \{ \sin(m\lambda-\omega t) [2\Omega(K_1-K_2) + K_1[\omega + \Lambda(2-m)]] - \alpha K_1 \cos(m\lambda-\omega t) \} - \alpha m K_1^2 (\cos\varphi)^{2m-1} [1+(1+m)\sin^2\varphi] \frac{\sin 2(m\lambda-\omega t)}{2}$$
$$+ \alpha K_1 (\cos\varphi)^{m+1} [(m\Lambda-\omega)\sin(m\lambda-\omega t) + \alpha \cos(m\lambda-\omega t)]$$
$$- \frac{\nu}{a} m(m+3) K_1 (\cos\varphi)^{m-1} \cos(m\lambda-\omega t) [(m+1)\cos^2\varphi - m],$$

$$G_v = \sin\varphi (\cos\varphi)^{m-1} [\alpha m \omega K_1 \cos(m\lambda-\omega t) + \alpha\alpha m K_1 \sin(m\lambda-\omega t)$$
$$- \alpha m^2 \Lambda K_1 \cos(m\lambda-\omega t) + 2\Omega K_1 \alpha m \cos(m\lambda-\omega t)$$
$$+ 2\alpha\Lambda K_1 m \cos(m\lambda-\omega t) - 2\Omega\alpha K_2 m \cos(m\lambda-\omega t)]$$
$$+ \sin\varphi (\cos\varphi)^{m+1} [-2\Omega K_1 \alpha m \cos(m\lambda-\omega t) - 2\alpha\Lambda K_1 \cos(m\lambda-\omega t)$$
$$- 2\alpha\Lambda K_1 \cos(m\lambda-\omega t) + 4\Omega\alpha K_2 \cos(m\lambda-\omega t) + 2\Omega\alpha K_2 m \cos(m\lambda-\omega t)]$$
$$+ \sin\varphi (\cos\varphi)^{2m-3} [-\alpha m^3 K_1^2 \cos^2(m\lambda-\omega t) - \alpha m^2 K_1 (m-1) \sin^2(m\lambda-\omega t)$$
$$+ \alpha^2 K_1^2 m^2 \cos^2(m\lambda-\omega t)] + \sin\varphi (\cos\varphi)^{2m-1} [\alpha m^3 K_1^2 \cos(m\lambda-\omega t)$$
$$+ \alpha m^2 K_1^2 \cos^2(m\lambda-\omega t) + \alpha m^2 K_1^2 \sin^2(m\lambda-\omega t) + (m-1)\alpha m^2 K_1^2 \sin^2(m\lambda-\omega t)$$
$$- 2\alpha K_1^2 m^2 \cos^2(m\lambda-\omega t) - 2\alpha K_1^2 m \cos^2(m\lambda-\omega t)]$$
$$+ \sin\varphi (\cos\varphi)^{2m+1} [\alpha K_1^2 m^2 \cos^2(m\lambda-\omega t) + 2\alpha m K_1^2 \cos^2(m\lambda-\omega t)$$
$$+ \alpha K_1^2 \cos^2(m\lambda-\omega t)] + \alpha\Lambda^2 \sin\varphi \cos\varphi$$
$$- \frac{\nu K_1}{a} m^2 (m+3) \sin\varphi (\cos\varphi)^{m-1} \sin(m\lambda-\omega t),$$

and

$$G_h = \frac{2\Omega a^2}{g} \sin(m\lambda-\omega t) [K_2\omega + \Lambda m (K_1-K_2) - m K_1 K_2 (\cos\varphi)^m \cos(m\lambda-\omega t)]$$
$$\times (\sin\varphi)^2 (\cos\varphi)^m.$$

With no friction ($\nu = 0$) the solution of the system (27) to (29), with the

initial condition given by (24) and (25), represents a wave which moves with angular phase speed ω without change in shape or amplitude. However, with friction, the wave will move with the same phase speed ω without change in shape but the amplitude for u and $-v$ will decrease according to the relation $A = A_o e^{-\alpha t}$, where A is the amplitude at time t and A_o is the initial amplitude. In fact, this is why we put the relation (26), because we know from section II.6.2 the effect of friction. The values used in the test experiment are

$m = 4$, (wavenumber 4),

$k = k_2 = \Lambda = 7.848 \times 10^{-6}$ sec^{-1},

$\Omega = 2\pi/86400$ sec^{-1},

$h_o = 3$ km,

$a = 6.4 \times 10^3$ km,

$g = 10$ m/sec^2.

III.2 Haurwitz wave initial condition

The initial field is non divergent, so that u and v can be derived from a stream function. In fact, we use the same stream function of the test experiment, or

$$\psi = a^2 K (\cos\varphi)^m \sin\varphi \cos m\lambda - a^2 \Lambda \sin\varphi .$$

The height field which balances this initial flow, or the height field which makes the time derivative of divergence initially zero is given by

$$gh = gh_o + a^2 A(\varphi) + a^2 B(\varphi) \cos R\lambda + a^2 D(\varphi) \cos 2R\lambda ,$$

where

$$A(\varphi) = \frac{\Lambda(2\Omega+\Lambda)}{2} C^2 + \frac{K^2}{4} C^{2m} \left[(m+1)C^2 + (2m^2-m-2) - 2m^2 C^{-2}\right],$$

$$B(\varphi) = \frac{2(\Omega+\Lambda)K}{(m+1)(m+2)} C^m \left[(m^2+2m+2) - (m+1)^2 C^2\right],$$

$$D(\varphi) = \frac{K^2}{4} C^{2m} \left[(m+1)C^2 - (m+2)\right],$$

and $C = \cos(\varphi)$.

The values used in the experiments are

$m = 4$ and 6, (wavenumbers 4 and 6),

$k = \Lambda = 7.848 \times 10^{-6}$ sec^{-1} ,

$\Omega = 2\pi/86400$ sec^{-1} ,

$h_0 = 8$ km ,

$a = 6.4 \times 10^3$ km ,

$g = 10$ m/sec^2.

Although the divergence and its time derivative is initially zero, significant divergence develops and thus the waves do not propagate with the Rossby-Haurwitz phase speed, nor do they mantain their shape precisely.

CHAPTER IV

EXPERIMENTS AND RESULTS

A basic mean flow, independent of longitude, superposed on it a disturbance will be integrated with time using equations (1) to (3). Two different types of disturbance are used, wavenumber four whose form changes a little during more than fifteen days of integration (stable wave), and wavenumber six which breaks down completely within few days forming cut-off lows and a region of zonal easterlies at about 50° N (unstable wave). Experiments with the following difference will be described

a. Runs with Fourier filtering.

b. Runs including the viscous terms in the momentum equations.

c. Runs which do not include either of the damping forces (a) or (b).

IV.1 Experiment notation

Hereafter we shall use the experiment notation AIIJJ(L-M), where

A stand for;

F if friction is used,

P if Fourier filter is used,

N if neither friction nor Fourier filter is used,

II is the number of grid points per latitude circle,

JJ is the number of grid points between the poles,

L will be used in case of friction and Fourier filter. In case of friction it indicates the value of kinematic viscosity used (ν), e.g. experiment including friction with $\nu = 10^{4}$ m^2/sec, L=4. Experiments with Fourier filter have L to indicate the value of the number of successive time steps used per M hours. If L and M are not included in an experiment notation for Fourier filter, this means that the 3-gridlength filter is used each time step.

For example in an experiment with II=32 and JJ=16,

the experiment notation is F3216(5) if friction is used with $\nu=10^{5}$ m^2/sec,

the experiment notation is P3216 if the Fourier filter is used each step,

the experiment notation is P3216(2-3) if the Fourier filter is used for two successive steps each three hours,

the experiment notation is N3216 if neither friction nor Fourier filter is included.

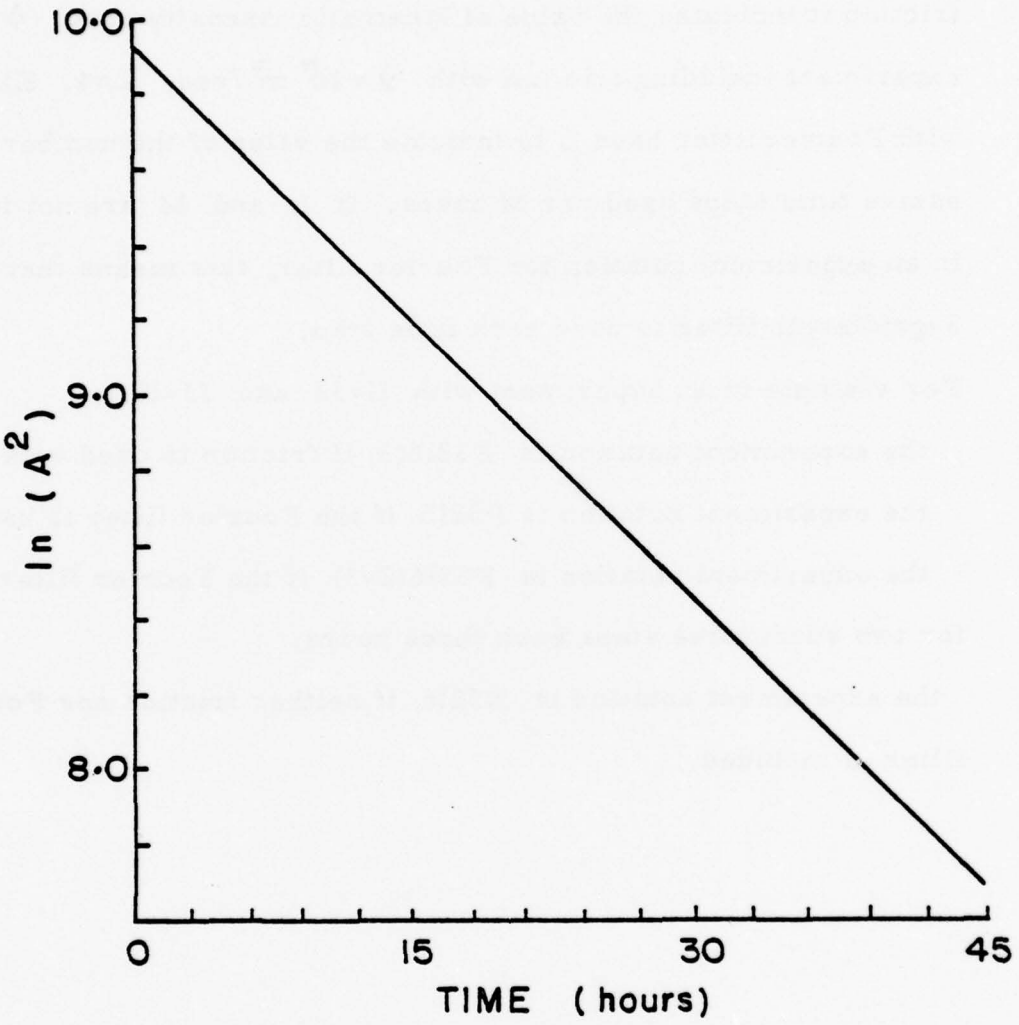

Fig. 1. The logarithm of the square of the amplitude of Fourier wavenumber 4 of the v-component of wind (summed for all grid latitudes) as function of time for the test experiment, F3216(7).

IV.2 Test experiment

It is essential before starting our experiments to be sure that the effect of including the viscous force, in the momentum equations, gives the expected results. In other words, it is important to test the program with and without this force for a simple initial condition to be sure that there are no programming errors or hidden instabilities.

The initial condition used in this test is Haurwitz initial condition for wavenumber four with the forcing function included as discussed in section III.1. This means that the model represent a non-divergent barotropic fluid for all times of integration. This means;

a. If the model runs without the viscous force, the result must be just a moving wave with known phase speed and without change of amplitude.

b. If the model includes the viscous force, then the u and v fields will move with the same phase speed but their amplitudes will decrease exponentially with time according to the equation, (see II.6.2)

$$A = A_0 e^{-\alpha t}, \quad \text{where} \quad \alpha = \nu\, m(m+3)/a^2.$$

The previous equation can be written as

$$\log (A)^2 = \log (A_0)^2 - 2\alpha t. \tag{30}$$

This means that the logarithmic change of the amplitude squared with time is linear with a slope of -2α. In this test experiment ν was taken to be 10^7 m^2/sec giving an e-folding time of roughly three days. The result for the experiment F3216(7) is shown in Fig.1. As expected from formula (30) a straight line resulted on a graph with the coordinate $\log (A)^2$ and t. From the graph the slope of the line $2\alpha = 0.137 \times 10^{-4}$

and from the values used $2\alpha = 0.1376 \times 10^{-4}$. In this experiment the time step used is 2 minutes. There was no evidence of any numerical difficulties.

IV.3 Experiments with wavenumber four

Hoskins (1973) has shown that a Haurwitz wavenumber four superimposed on a constant angular velocity zonal flow is stable in the sense that the wave propagates in an east-west direction with little change in shape. In other words, there is little cascade of energy or enstrophy during a time integration. As such, one expects that there will not be a serious difficulty in the simulation of this wave from the point of view of the control of aliasing instability. Indeed we have found that an integration with low resolution (II=32 and JJ=16) can proceed for 16 days without any controls at all. On the other hand, the inclusion of filtering or a friction term while permitting a longer integration time has, surprisingly, rather significant effects on the nature of the solution. In this section we describe the result of experiments with low resolution and high resolution (II=64 and JJ=32). We found that the main wave moves eastward with faster speed for high resolution experiments. Its displacement varied between 10.7° per day and 11.4° per day compared to the 12.2° per day predicted by the nondivergent theory*. The phase speeds obtained here do not contradict

* As shown by Haurwitz (1940), in a nondivergent barotropic atmosphere the flow pattern moves from west to east without change of shape with the angular velocity v, where

$v = [R(R+3)\omega - 2\Omega]/(1+R)(2+R)$, the symbols as in III.2.

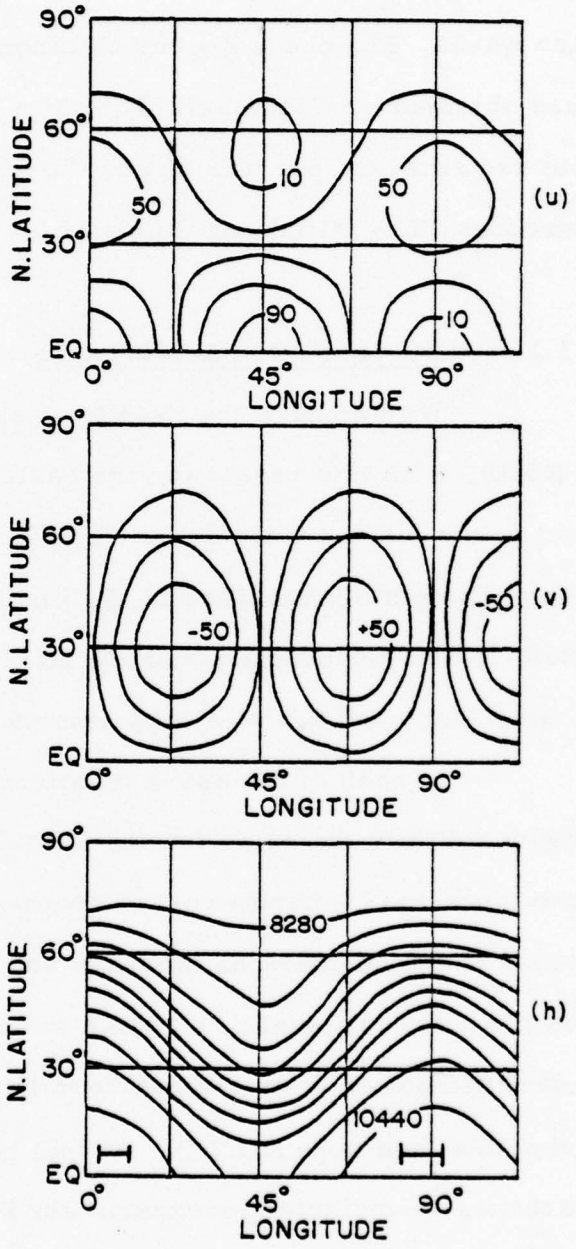

Fig. 2. Initial conditions (Haurwitz wave 4); u(m/sec) v(m/sec) and geopotential height h(meters) with interval 240 meters.

those obtained by Bourke(1972) and Merilees (1974), as some of the constants are different with the result that in these experiments we get faster waves. The phase speeds obtained here are very similar to the values obtained by Hoskins (1973), while the values obtained by Phillips (1959) are smaller, perhaps due to the use of second order finite differences. The initial conditions of u, v and h are shown in Fig.2.

IV.3.1 Low resolution experiments

We compare the results of experiments F3216(5), P3216(1-3) and N3216. With this resolution the basic disturbance is described by 8 grid points along a latitude circle. The maximum zonal wavenumber which is completely resolved is 15. The filter used in the experiment P3216(1-3) will periodically remove all wavenumbers greater than 10. The time step used in these experiments is 10 minutes.

In each of the above mentioned experiments, the behaviour was substantially the same for the first 3 or 4 days. The disturbance quickly developed a north-west to south-east tilt in the northern latitudes of the northern hemisphere and a north-east to south-west tilt in the polar latitudes. This has the effect of transporting westerly angular momentum from the northern latitudes towards both the equator and the pole (see appendix III). At this point, the behaviour of the disturbance as indicated by experiment P3216(1-3) begins to differ from the other two experiments. In the experiment P3216(1-3) the wave tilt developed initially is maintained whereas in the other experiments the wave tilt reverses. These results are shown in Fig. 3(A)

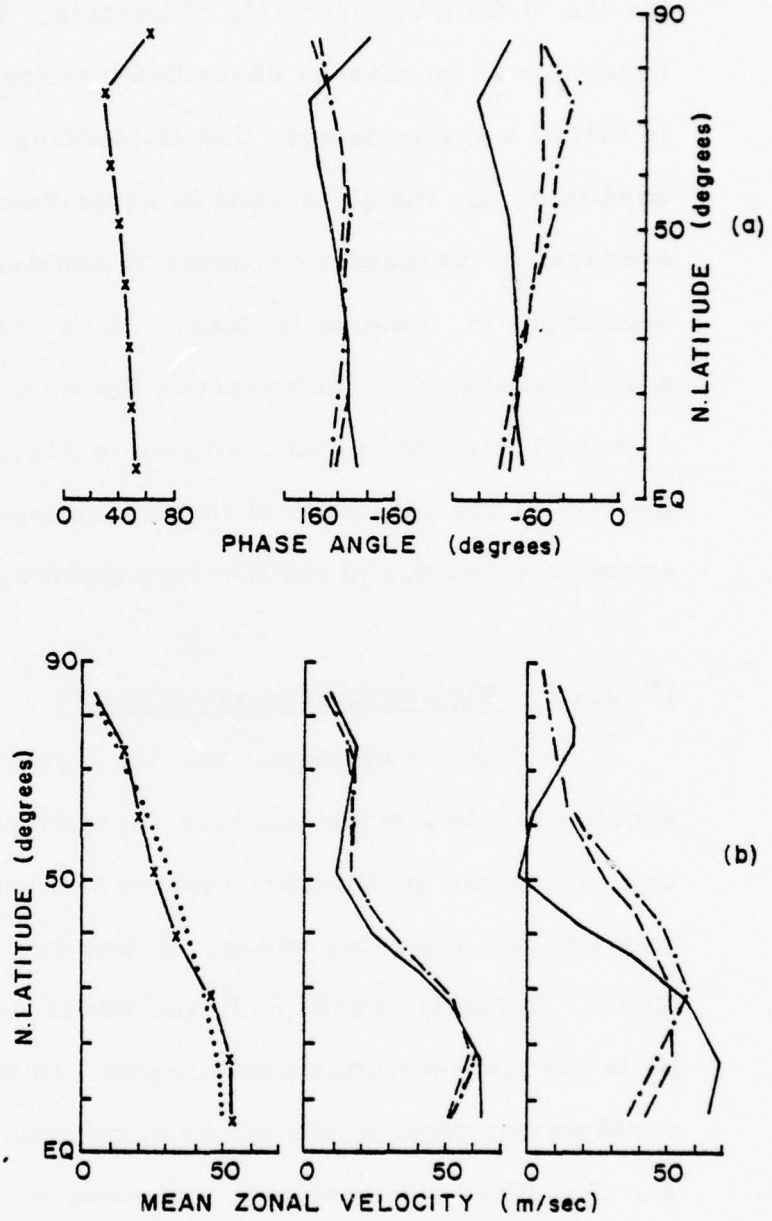

Fig. 3. Latitudinal distributions of phase angle (A) and longitudinal zonal velocity (B) on the days 3, 6 and 9 (from left to right) for the experiments P3216(1-3) (solid line), F3216(5) (dash line) and N3216 (dash-dot line). Dash-cross line used when the experiments are about the same. Dotted line for initial profile

where we have plotted the phase of the main disturbance (wavenumber 4) for the v-field as a function of latitude. The figure indicates that the behaviour of the flow as described by experiments N3216 and F3216(5) is that of a stable nature, that is, tending to return to the initial condition. On the other hand in experiment P3216(1-3), the zonally averaged u-component continues to accelerate in low latitudes and decelerate in middle latitudes. As a result the distribution of the zonally averaged u-component of the wind is completely different after 9 days of integration as indicated in Fig.3B. As we shall show presently, the behaviour of the experiment P3216(1-3) appears to be anomolous and due to the filtering applied.

IV.3.2 High resolution experiments

Since we expect that the higher resolution experiments should provide a more accurate approximation to the true solution, we are able to use such experiments to tell which of the low resolution experiments are going wrong. In this section, we compare experiments N6432, F6432(5), P6432(2-3)* and P6432 for the same initial conditions as in the low resolution experiments. In this grid system the maximum zonal wavenumber which can be completely represented by the grid is 31. The filter when applied, will remove wavenumbers greater than 20. The time step used in these experiments is four minutes.

---

* Experiment P6432(2-3) is discussed and not P6432(1-3) because, as we shall see in section IV.3.3 experiment P6432(1-3) exites the two time step computation mode.

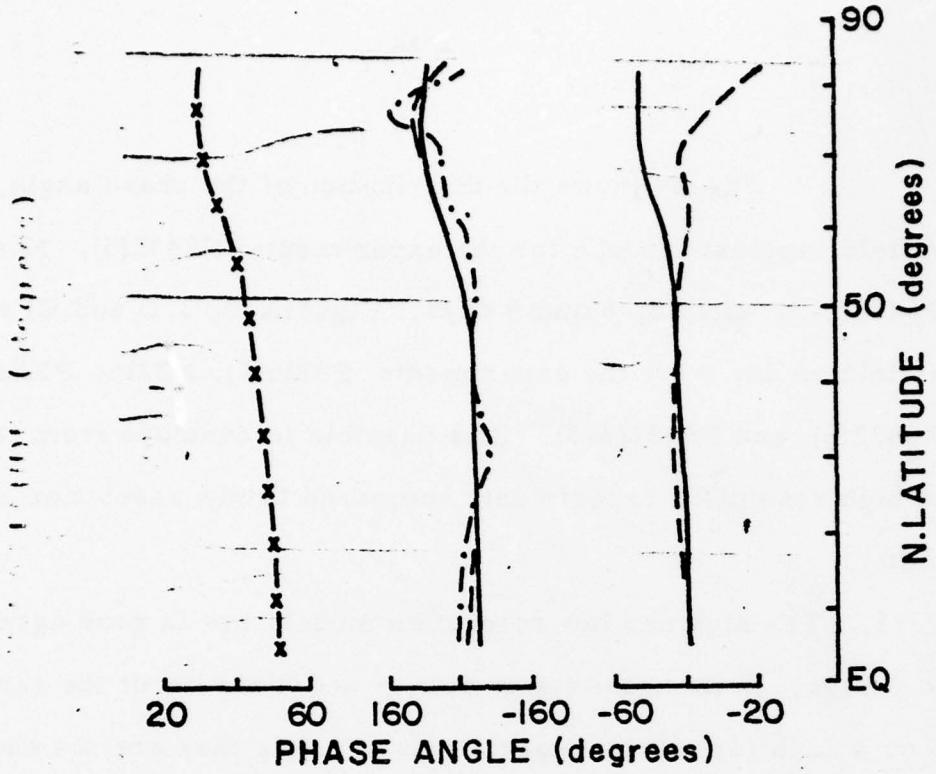

Fig. 4. Same as Fig.3(A) except for high resolution experiments.

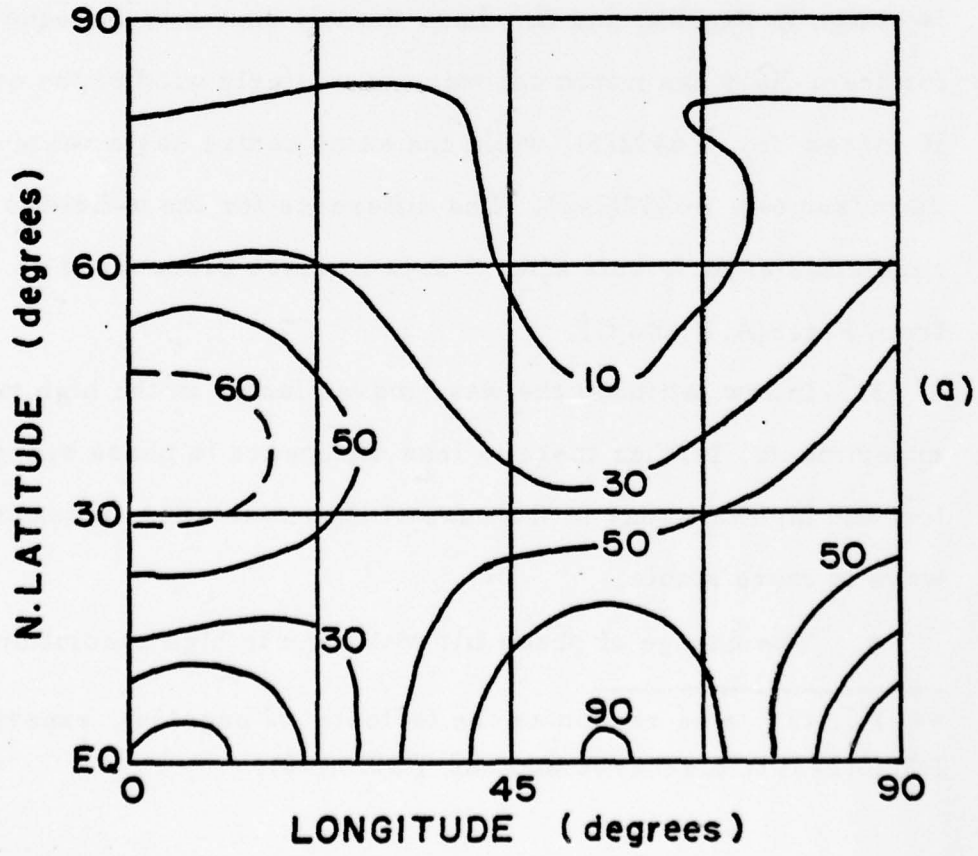

Fig. 5. Isopleths for the u-field, on day 9, for the experiments F3216(5), N3216, P3216(2-3), F6432(5) and P6432(2-3); A, B, C, D and E respectively.

Fig.4 shows the distribution of the phase angle, for the ν-field, against latitude for the experiments F6432(5), N6432 and P6432(2-3) after 3, 6 and 9 days. Fig.5(A, B, C, D and E) shows the u-field on day 9 for the experiments F3216(5), N3216, P3216(2-3)**, F6432(5) and P6432(2-3). It is possible to conclude from the results of high resolution experiments compared to low resolution experiments that;

1. The high and low resolution models are in good agreement up to 3 days. In fact, the fields of u, ν and h are about the same up to 3 or 4 days for all the experiments and thus they are not shown.

2. The high resolution models generally give the same results up to 9 days. There are some differences, the most noticible of which is shown in Fig.5(D and E) where the low centre in the equatorial area for the u-field has minimum value of westerly wind of the order of 10 m/sec for F6432(5), while the same centre has a value of about 30 m/sec for P6432(2-3). The difference for the u-field for low resolution experiments after 9 days is more pronounced as is clear from Fig.5(A, B and C).

3. In low latitudes the wave moves faster in the high resolution experiments, further there is less difference in phase speed between low and high latitudes in the case of high resolution indicating that the wave is more stable.

4. The change of phase tilt with time in high resolution experiments

---

** For the same reason as the footnote of page(34), experiment P3216(2-3) is discussed and not P3216(1-3).

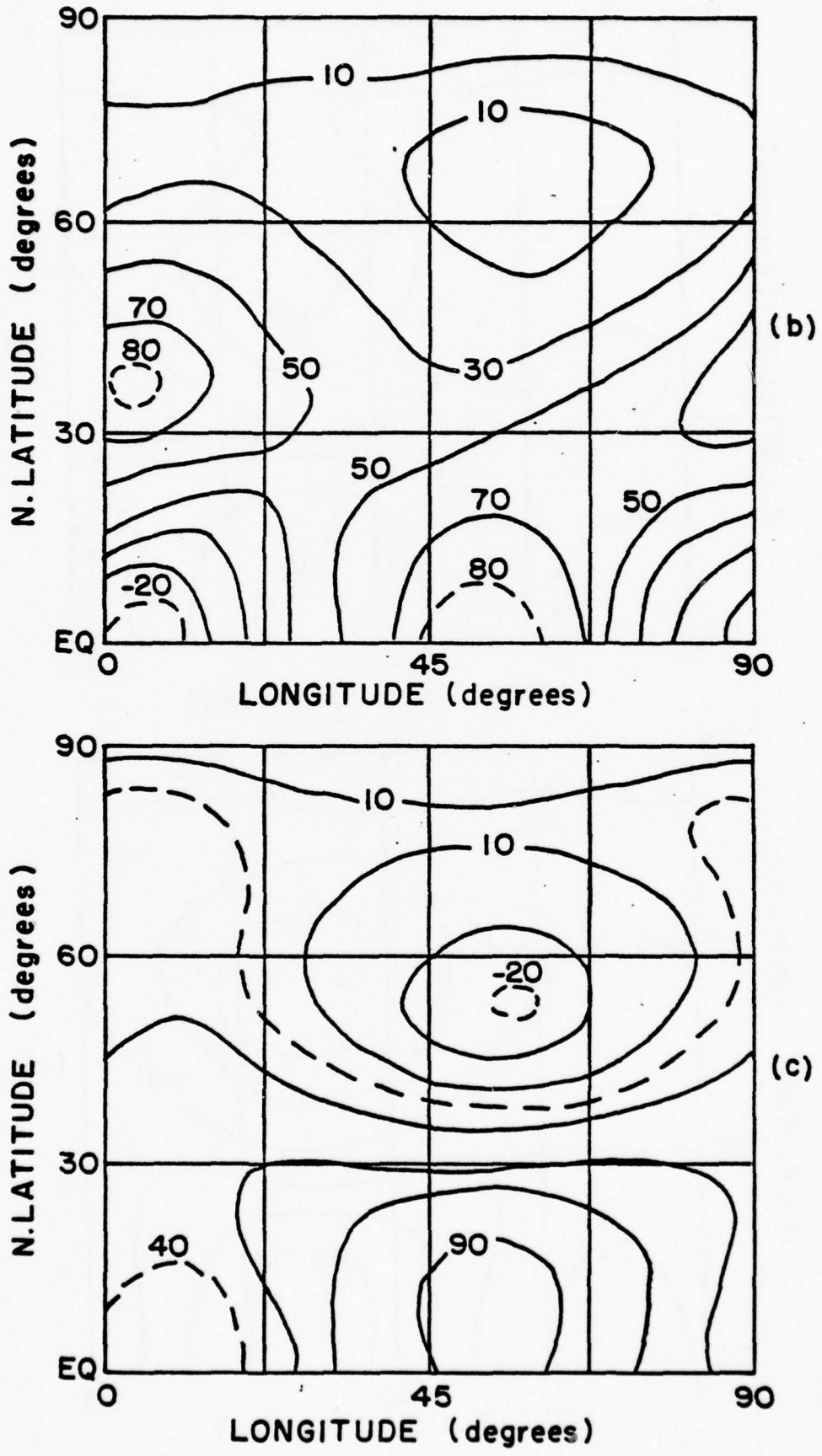

Fig. 5 (continued from p. 35)

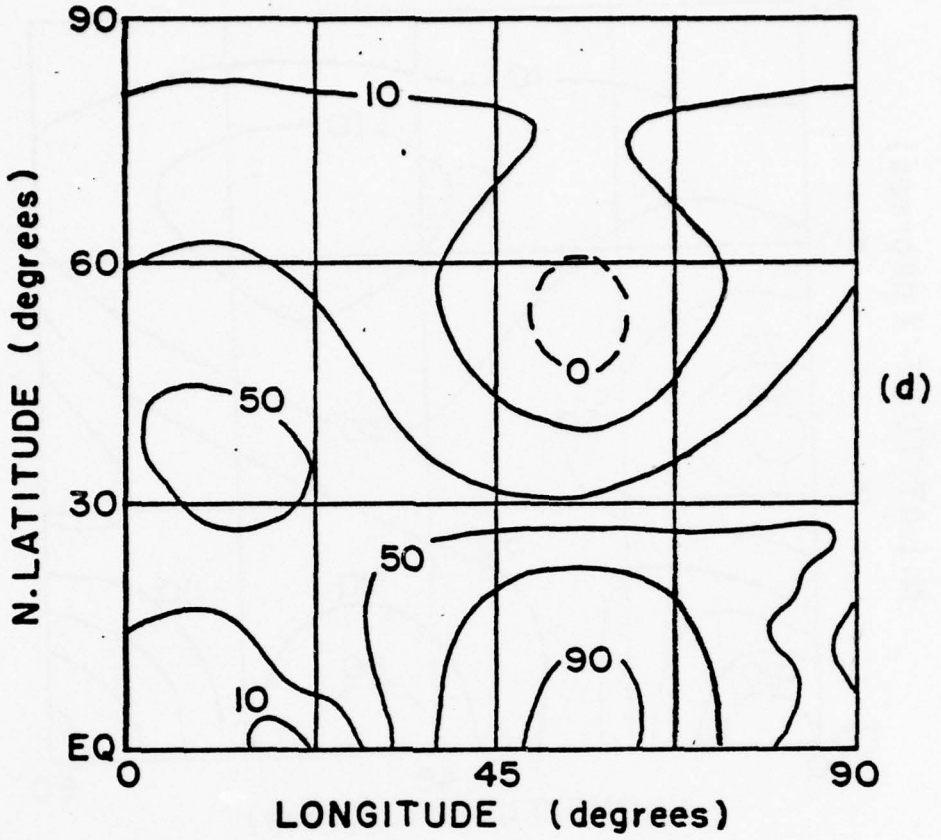

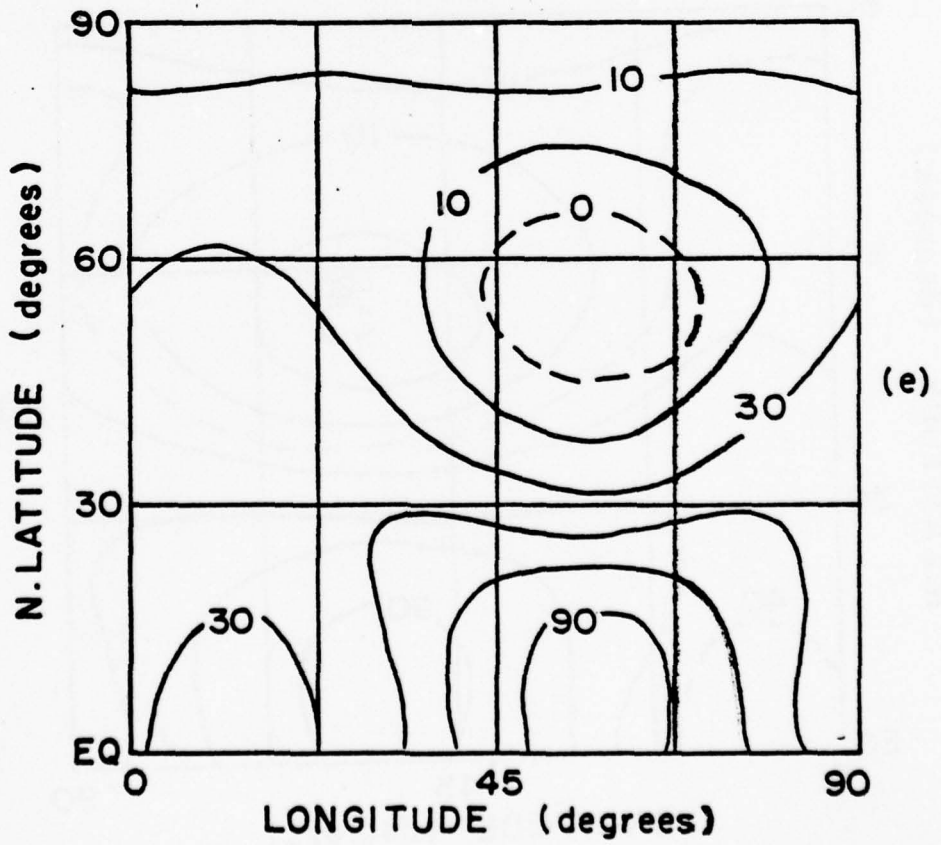

Fig. 5 (continued from p. 37)

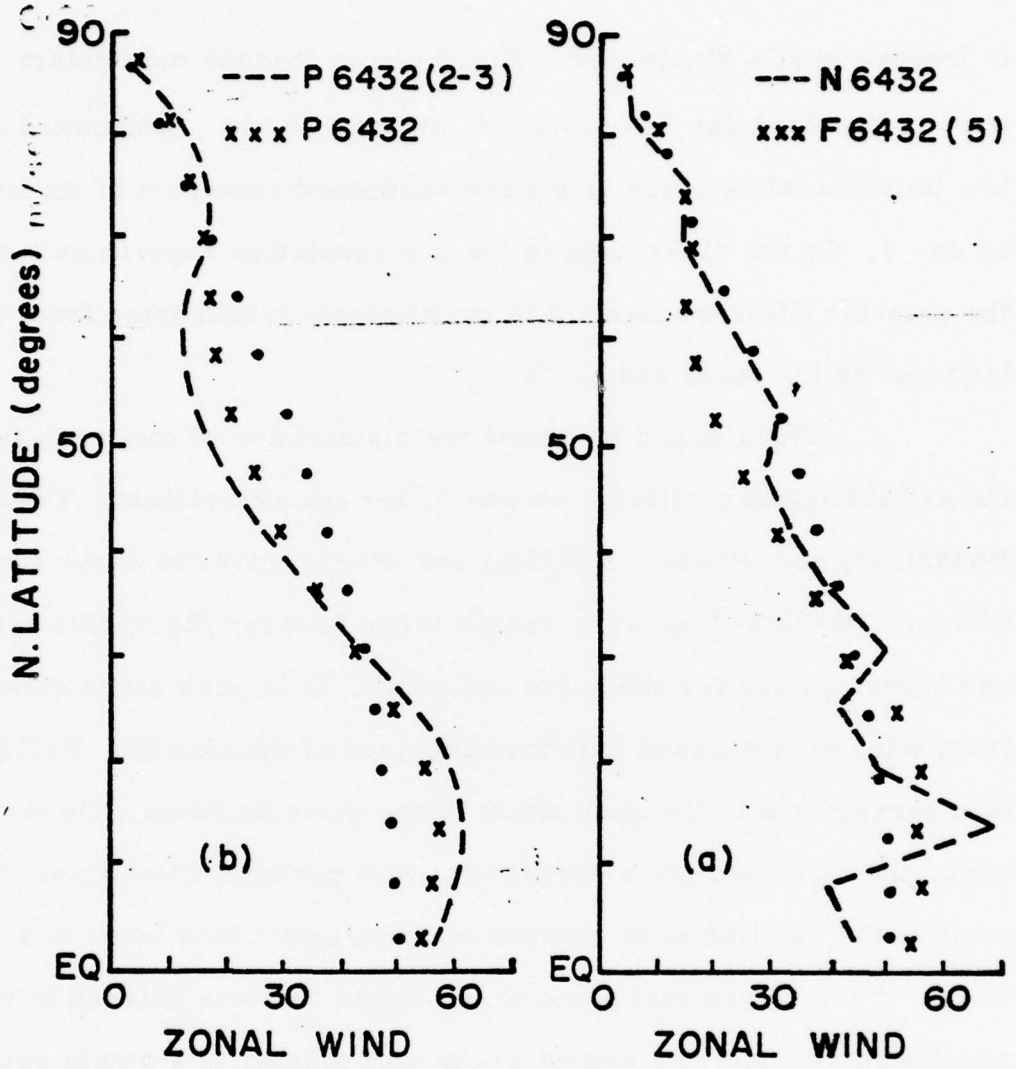

Fig. 6. Comparison of the zonal average of the u-component of wind (m/sec) after 9 days except for N6432 (after 8 days), as function of latitude; dotted line is the initial profile.

is indicative of a stable flow. Fig.4 shows that the momentum transport on the third day is southward, on day 6 is northward from low latitudes while there is a weak southward transport of momentum on day 9. On the other hand in the low resolution experiments with the periodic filter, momentum is continuously transported from middle latitudes to the north and south.

Fig.6(A and B) shows the distribution of the mean flow for the u-field against latitude, on day 9, for the experiments F6432(5), P6432(2-3) and P6432. F6432(5) and P6432 give the same distribution but P6432(2-3) gives a weaker mean flow for the middle latitudes and higher values for the north and south. It is possible to conclude from what we discussed that the behaviour of the flow for P3216(2-3) is incorrect due to the application of the periodic filter. On the other hand, the high resolution experiment with periodic filtering is able to capture the oscillation in momentum transport which leads to a stable wave. We conclude that some of the waves that are filtered in the low resolution experiments are essential components of a stable oscillation.

When no smoothing is applied to the high resolution experiments the calculation " blows-up " after about 8 days. Note the noise on the distribution of the mean flow as shown in Fig.6(A). We can also see irregularities in low latitude in the u-field as shown in Fig.5(D). The problem of instability will be discussed further in section IV.3.4.

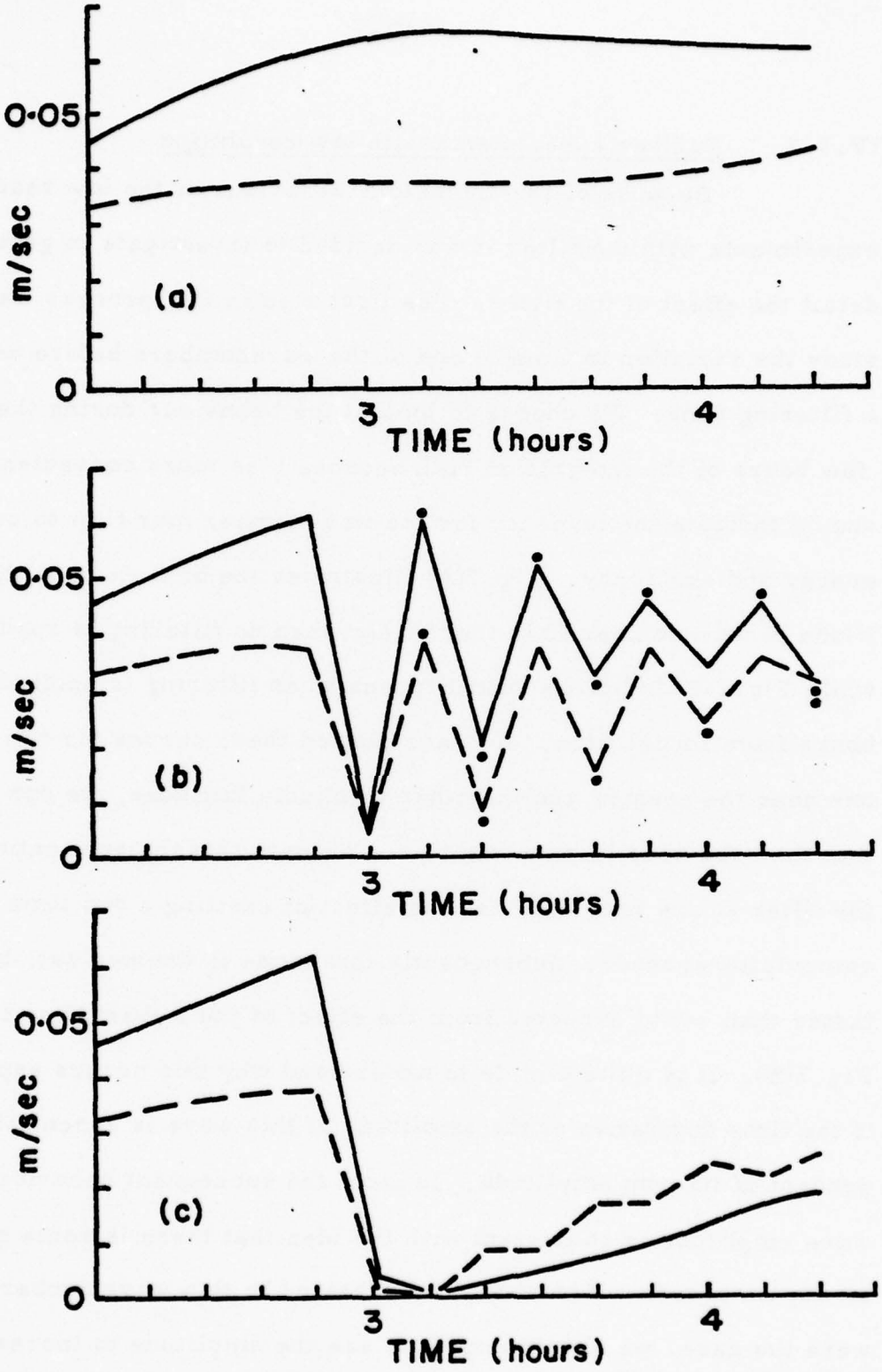

Fig. 7. The amplitude of wavenumber 12 of the v-component of wind as a function of time at two latitudes. Solid lines are for 5.6°N and dotted lines for 39.3°N. The upper figure (A) corresponds to the experiment N3216, the middle (B) to P3216(1-3) while the lower (C) to P3216(2-3). The circles on (B) represent the experiment without Robert time filter.

IV.3.3 Further experiments with low resolution

Because of the anomalous behaviour of the low resolution experiments with the filter it was decided to investigate in greater detail the effect of the filter. The first step in this process was to study the variation in time of one of the wavenumbers before and after a filtering time. We choose to look at the behaviour during the first few hours of the integration both because it is more convenient and it should indicate the tendency for the wavenumber four flow to cascade energy and enstrophy. Fig.7(A) illustrates the behaviour of the amplitude of wavenumber 12 in the v-field when no filtering is applied while Fig.7(B) indicates what happens when filtering is applied at 3 hours from initial time. We have plotted these curves for two latitudes, one near the equator and the other in middle latitudes, we can see that the behaviour is quite similar. We note that the application of the filter at one time step has the effect of exciting a two time step computational mode. Subsequently this mode is damped out, but much faster than would expected from the effect of the Robert time filter, Fig.7(B). It is quite simple to understand why this occurs especially if the time derivative of the amplitude of this wave is essentially independent of its own amplitude. In fact, the subsequent behaviour of the wave amplitude is consistent with the idea that there is some quasi-steady amplitude which should be acheived in this wavenumber. If that were the case, we should expect to see the amplitude to increase when it is excessively low and remain about the same level where it is before filtering. These ideas are further supported by the curves in Fig.7(C)

which show the result of applying the filter on two successive time steps. Note how the two time step oscillation is considerably reduced. Further, the amplitude of the wave tends to grow back to its level before filtering. This indicates that energy will tend to flow to this wave when it has little. Since it is, in general, good practice to minimize the exitation of two time step oscillation it was decided that it would be better to apply the filtering on two successive time steps*.

One of the rather arbitrary features of the application of the filter is how frequently it is applied. Some very rough experiments by Merilees (1974) suggested that every three hours was alright, but no serious effort was made to investigate it more thoroughly. Here we carried out a number of experiments to see how the solution changes as we change the frequency of the application of the filter.

We first compared the effects of filtering at two successive time steps every three hours and every hour with filtering once every three hours. Fig.8(A) shows the distribution of the phase angle of zonal wavenumber four of the ν-field. We note that the tilting of the phase is less pronounced when we filter every hour. Filtering at two successive time steps every three hours tends to produce slightly less tilt but the distribution of phase is quite similar to that obtained by filtering once every three hours. In Fig.8(B) we show the zonal component of the u-field after 9 days and we can see the effects of the

---

* This practice is apparently well known by those who have experience in grid point models. However, people who work with spectral models have generally not concerned themselves with it.

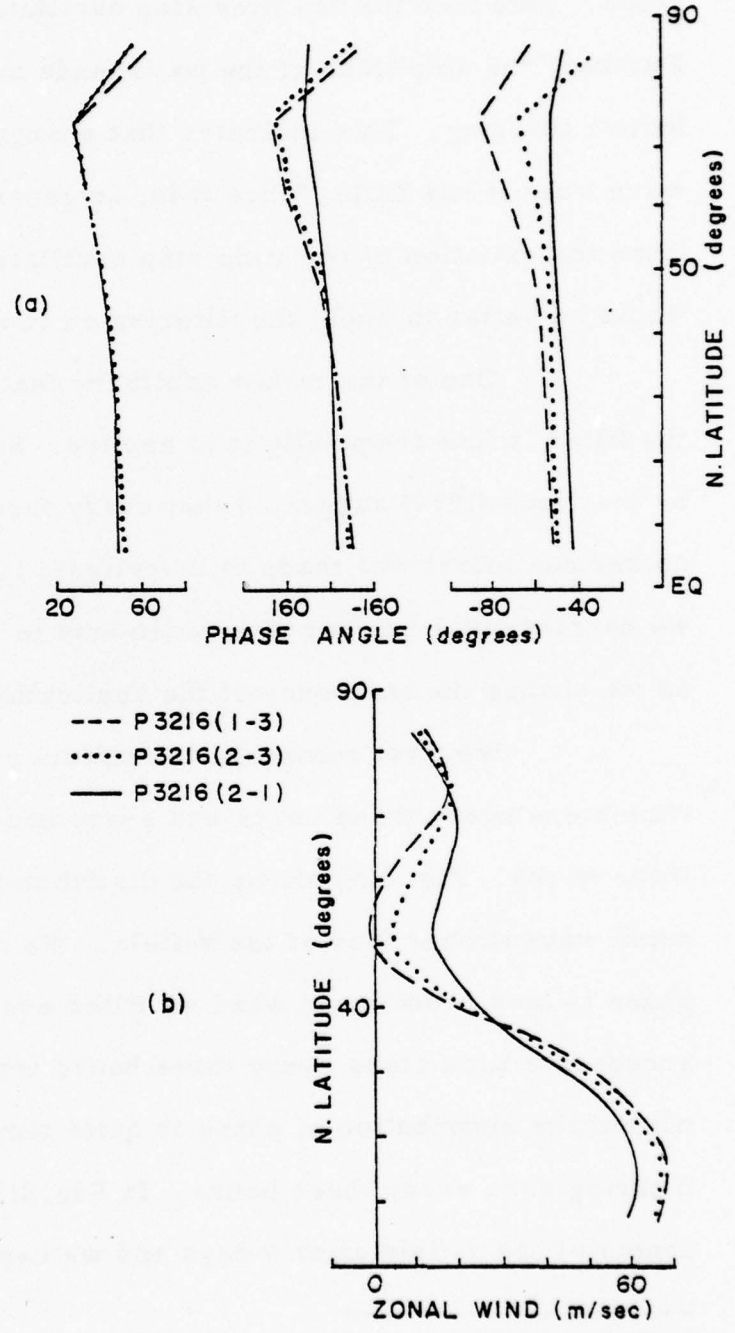

Fig. 8. A: The phase angle of wavenumber 4, for the v-field, as function of latitude after 3, 6 and 9 days (from left to right). B: The corresponding zonal average of the u-field after 9 days.

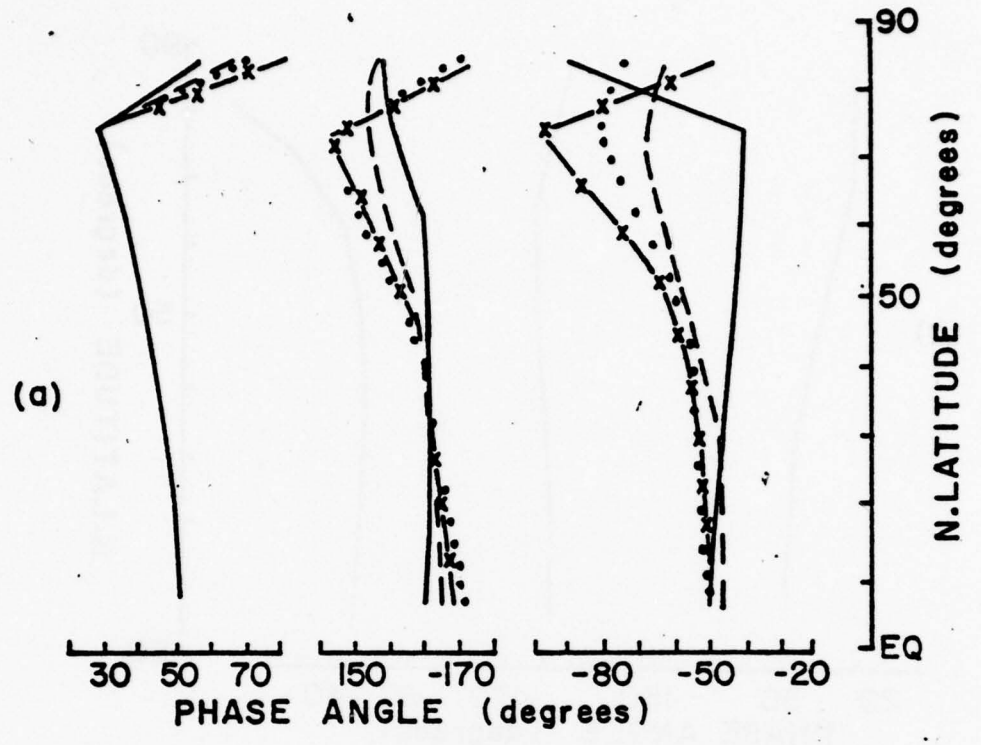

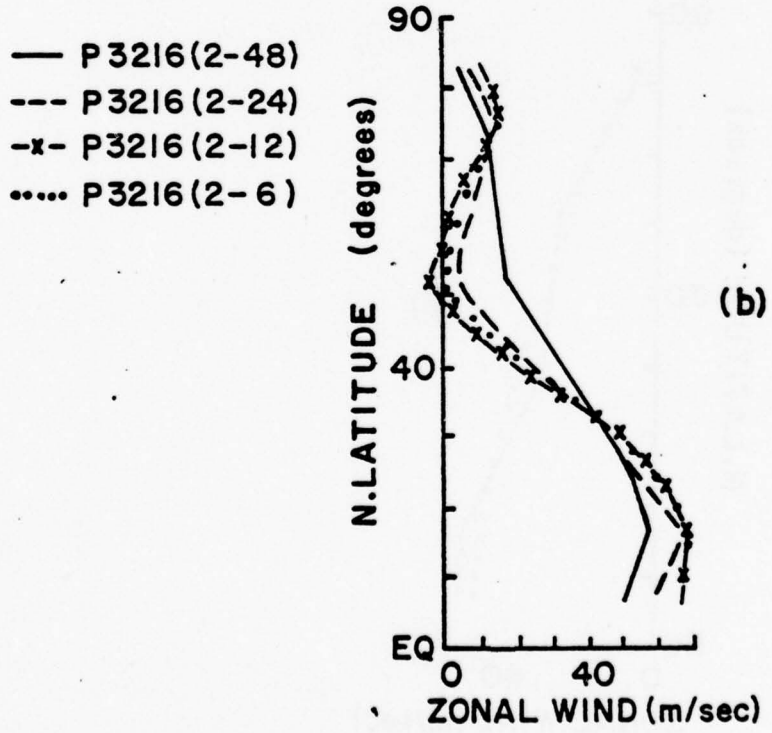

Fig. 9(A and B). Same as Fig. 8(A and B)

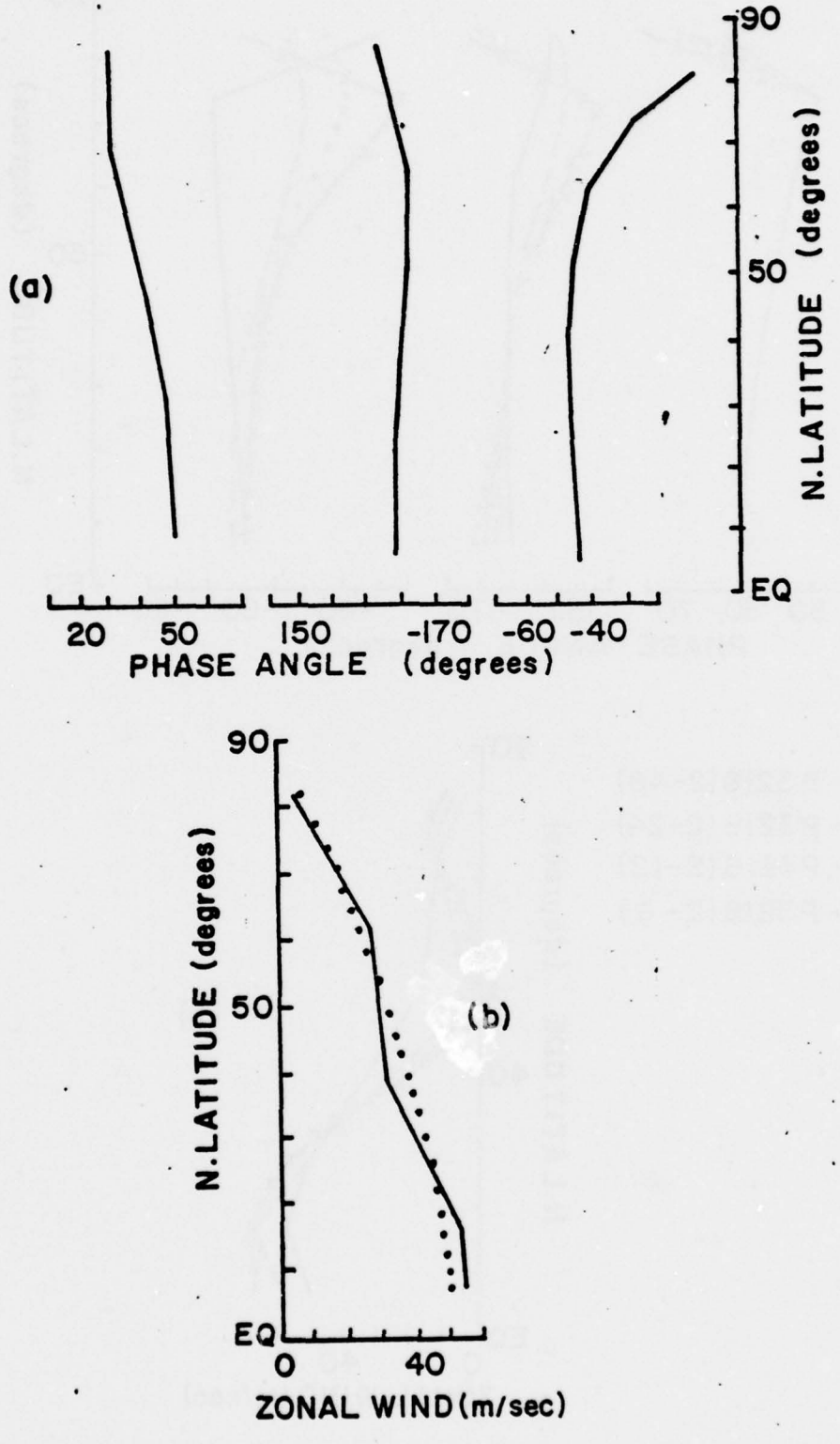

Fig. 10. Same as Fig. 8 but for the experiment P3216. Dotted line is the initial profile.

tilting of the phase lines. While there are some differences caused by the double application of the filter at three hour intervals, the interval of time between the application of the filter appears to be more important. Based on this consideration a number of experiments were performed in which the time interval between application of filter was varied between zero and 48 hours. In each of these experiments the filter was applied at two successive time steps. Interestingly, we find that the tilting of the phase of the wavenumber four of the v-field is not monotonically dependant on the time interval between application of the filter. In fact, the application of the filter at 12 hours intervals appears to produce the maximum effect as shown in Fig. 9(A). Naturally, a similar effect is produced on the profiles of the zonally averaged component of the u-field as shown in Fig. 9(B). Using the filter each time step, surprisingly, showed the more stable solution, Fig. 10(A and B), with the least change of energies. Fig. 11 shows the kinetic and potential energies as well as their sum during a period of 13 days for the low resolution experiments. The figure shows a change of less than 2% in the kinetic energy for the experiment P3216 during the 13 days of integration.

As a convenient summary of the sort of results obtained we present Fig. 12. The ordinate is the difference between the zonally averaged u-field after 9 days of integration and the initial value of this same field at about 51° N. Since the true solution oscillates about the initial conditions, this provides a measure of error. Along the abscissa we plot the different experiments in order of decreasing time

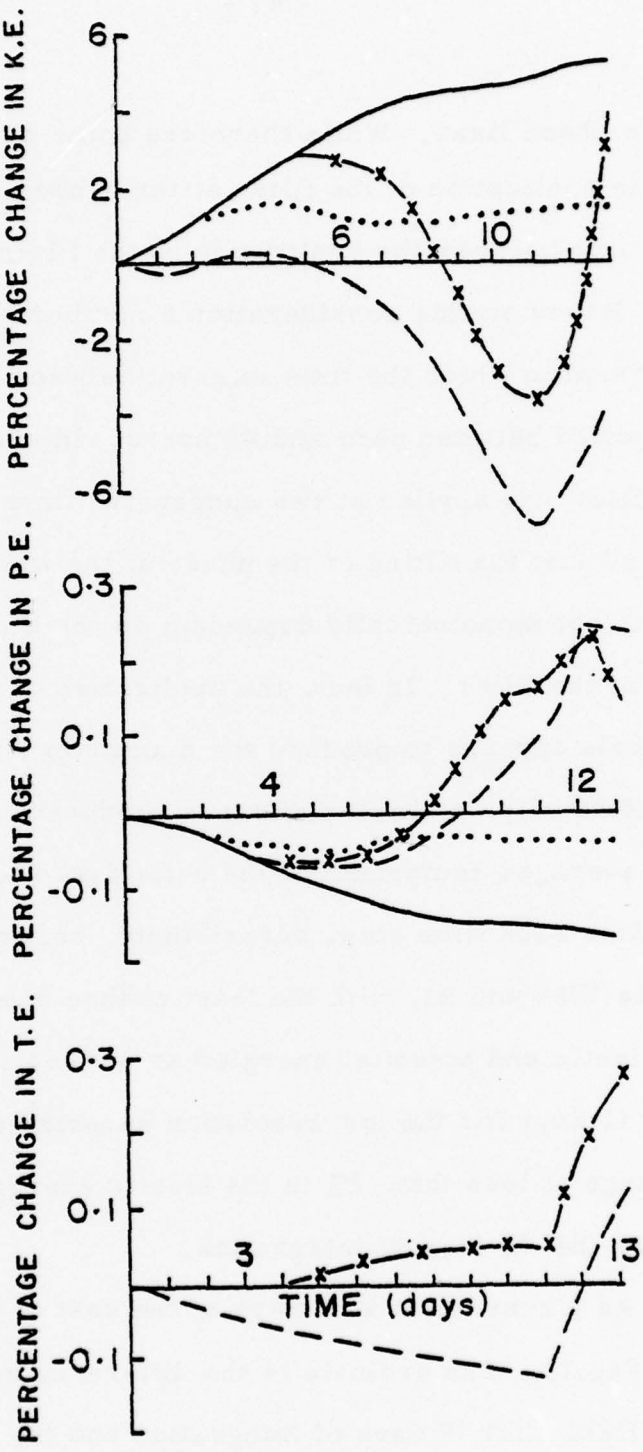

Fig. 11. The percentage change from initial time of the Kinetic Energy (K.E.), Potential Energy (P.E.) and the Total Energy (T.E.) for the experiments N3216 (dash-cross lines), F3216(5) (dash lines), P3216(2-3) (solid lines) and P3216 (dotted lines), as function of time.

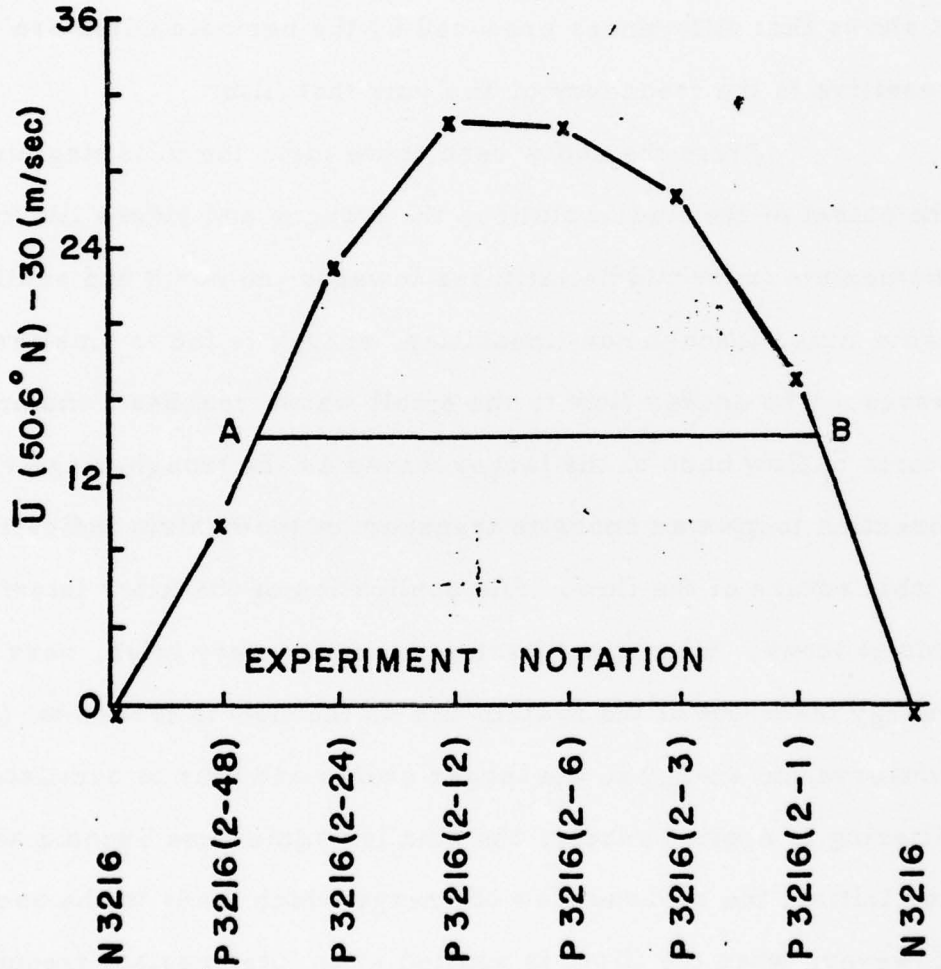

Fig. 12. The difference between the mean zonal flow $\bar{U}$ at about 50.6°N, on day 9, and 30 m/sec for different experiments.

interval between application of the filter. While the diagram indicates similar difference in the zonally averaged u-field for intervals of time corresponding to points A and B, the details of the simulation are, in general, different. A more important conclusion from Fig.12 that, it shows that differences produced by the periodic filter are very sensitive to the frequency of applying that filter.

From the above results we form the following picture. At the outset of the flow evolution, the troughs and ridges tilt to transport momentum from middle latitudes towards the north and south. At the same time, through non-linearities, energy is fed to smaller scale waves. The energy flow to the small waves reaches a maximum then starts to flow back to the larger waves as the trough-ridge tilt reverses direction to give an opposite transport of momentum indicative of the stable nature of the flow. The application of the filter interferes with this process. When the filtering is applied very often, very little energy leaks out of the system and so the flow is forced to (almost) conserve the energy in the larger scales and thus to oscillate. If the filtering is applied rarely, the smaller scales can become saturated and initiate the reverse flow of energy which leads to the oscillation. However, when the filter is applied at an intermediate frequency, a significant amount of energy is removed from the system at the small scales, and the large scales will tend to feed still more energy to these scales much as though the integration were beeing restarted after each filtering.

Since the process of an oscillating tilt must be related to

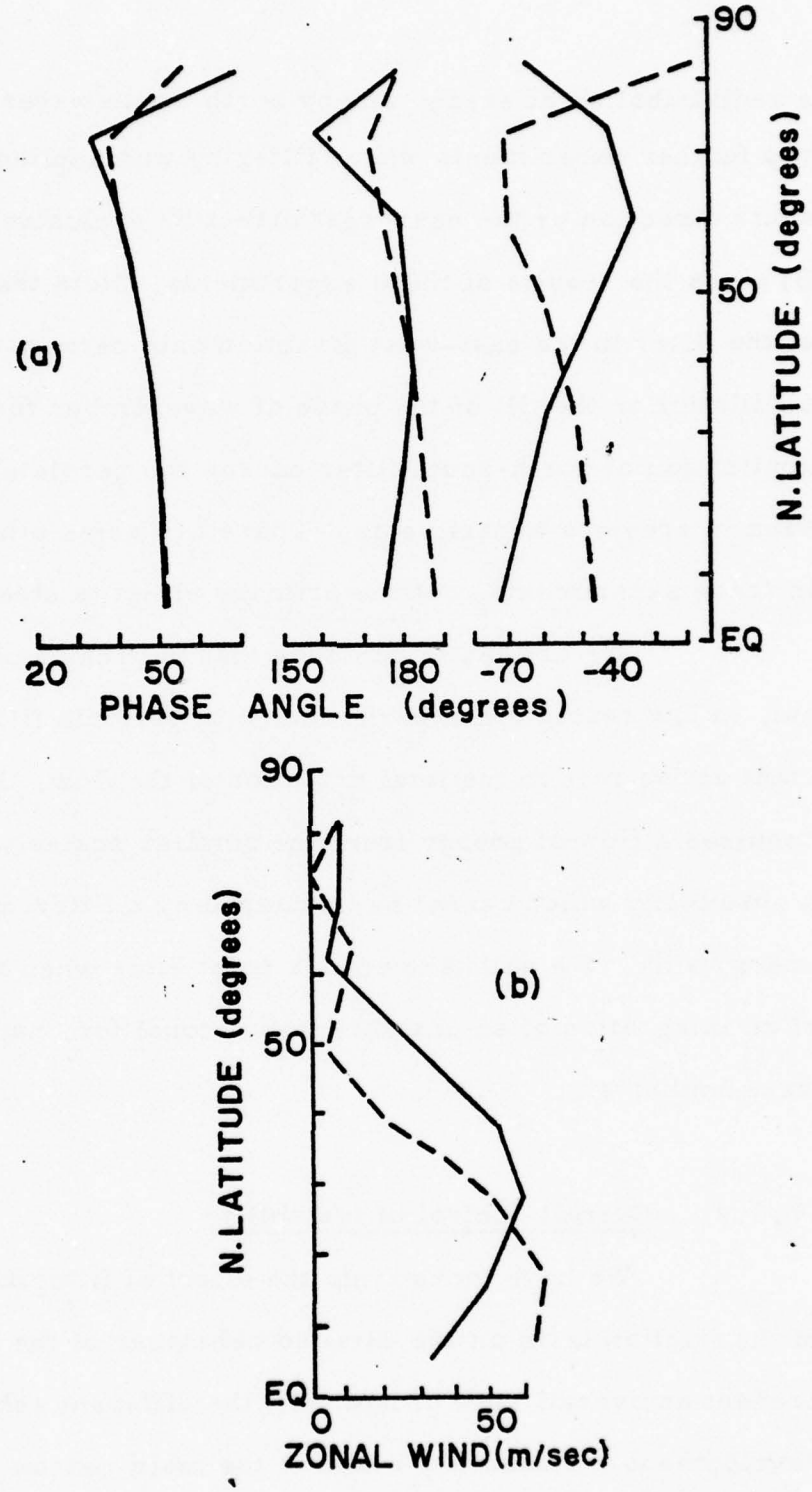

Fig. 13. Same as Fig. 8 except for the experiment P3216(2-3) with east-west filtering (solid line) and north-south filtering (dashed line).

a redistribution of energy among north-south waves we carried out two further experiments where filtering was applied either in the north-south direction or the east-west direction exclusively. Fig.13(A and B) gives the results of these experiments. Note that the application of the filter in the east-west direction only permits the appropriate oscillation in the tilt of the phase of wavenumber four whereas the application of north-south filter causes the persistent tilt that has been seen in previous experiments. There are some other effects going on in these experiments, but the primary effect is clear.

We are led to conclude that the scales of motion filtered out, in low resolution experiments with periodic filter, play an important active role in the total evolution of the flow. Further, the process requires a flow of energy from the smaller scales to the large scales a possibility which cannot be envisaged by a filter which serves as an energy sink. We will take up this point later when we discuss the result of an integration of an unstable initial condition, namely, Haurwitz wavenumber six.

IV.3.4 Overall control of instability

We have looked into the effect of filtering and the inclusion of the friction term on the detailed behaviour of the flow. Here we present an overall view of how well the different schemes control the development of instability which is the main reason for including friction or filtering. Table 3 indicates to the nearest day how long a particular integration proceeded before numerical instability developed.

We note, from Table 3, that the use of the 3-gridlength filter extends the calculation as far as our longest run without indication of any instability. In the experiments with a friction term, three values of kinematic coefficient of viscosity were tried; $\nu 1=10^4$, $\nu 2=10^5$ and $\nu 3=10^6$ m^2/sec.* In the low resolution experiments, the low value of

TABLE 3.

Experiment notation	No. of days before "blow-up"	Experiment notation	No. of days before "blow-up"
N3216	16	N6432	8
F3216(4)	17	F6432(4)	9
F3216(5)	18	F6432(5)	12
F3216(6)	>20	P3216(2-3), P6432 P6432(2-3) and P3216	>20

friction managed to delay the numerical instability for less than one day. The medium value of friction was sufficient to add another day of simulation. The high value of friction controlled the instability to the 20 day limit of integration, but produced far too much smoothing.

---

* In middle latitudes for high resolution experiments and with mean flow of 30 m/sec $\nu 1$, $\nu 2$ and $\nu 3$ give values for the local Reynold's number of the order 10^3, 10^2 and 10 respectively.

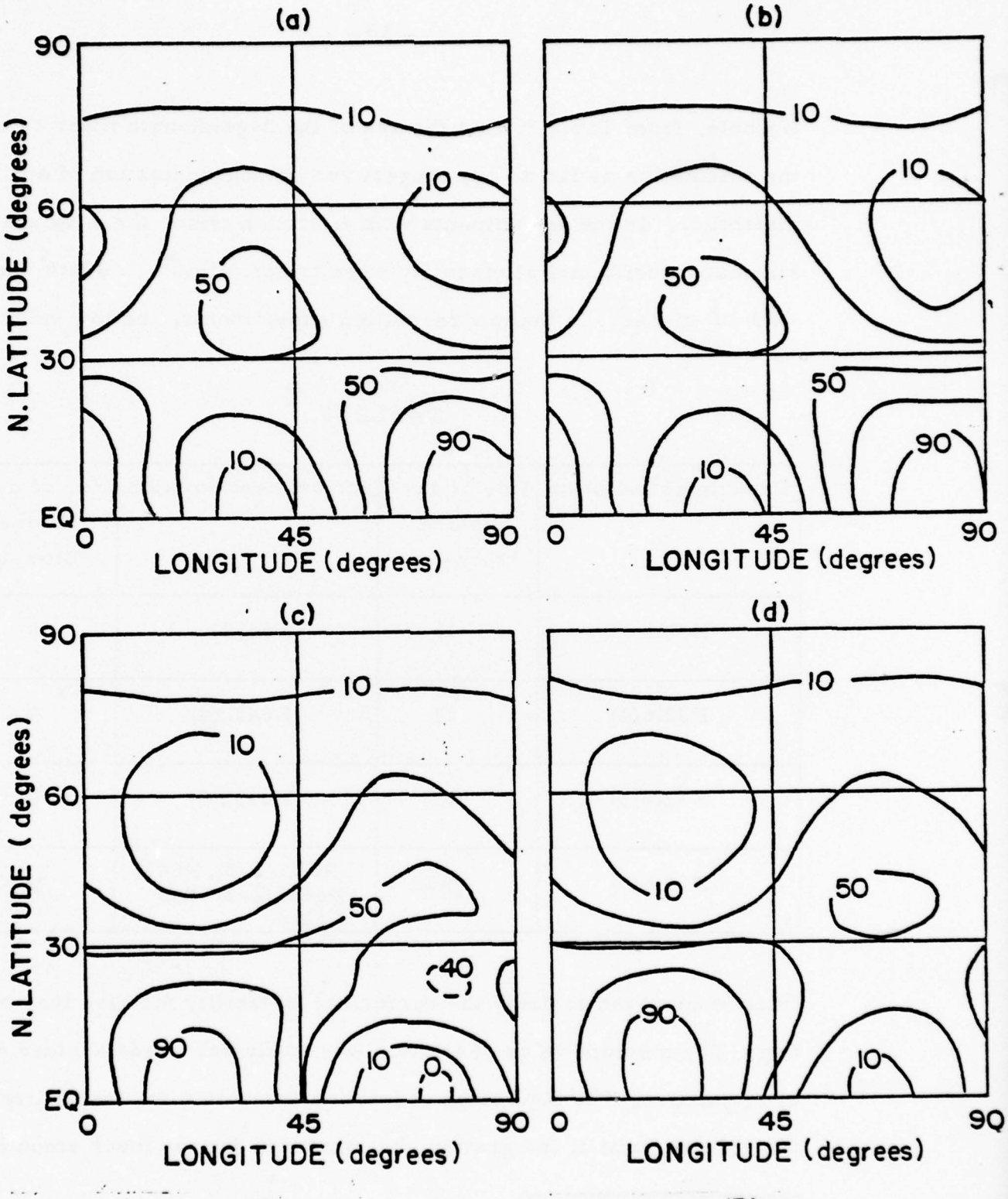

Fig. 14. The u-fields (m/sec) on day 3 (A and B) and on day 6 (C and D) for the experiments N6432 and F6432(5) respectively.

In fact, after 10 days with high friction coefficient the amplitude of wavenumber four for the v-field at about 28.1°N (the maximum value) decreases to about 47% of its initial value and to 63% after 15 days, while without friction the same point decreases by less than 2% after 15 days for P3216 and less than 0.002% for P6432.

Fig. 14(A, B, C and D) shows the u-field on the days 3 and 6 for the experiments N6432 and F6432(5). The two models are very similar up to 3 days without indication of instability. On day 6 irregularities are apparent in low latitudes in experiment N6432. In fact, some indication of irregularities could be seen as early as day 4. These irregularities grow rapidly with time and cause a "blow-up" on day 8. The experiment N6432 was repeated with half the time step (Δt=2 minutes), but the same instability appeared at the same time ending the calculation on the same day. F6432(5), on the other hand, has no indication of instability on day 6. It is clear, apart from the areas of irregularities, that F6432(5) and N6432 are in good agreement on day 6. Fig. 5(D) shows the u-field on day 9 for the experiment F6432(5). The appearance of a similar irregularities is shown in the u-field of that day. The growth of these irregularities causes the "blow-up" of calculation on day 12.

The instability of the low resolution experiments appears to be different. The first indication of trouble can be noticed as early as day 10 at which time significant amplitude is contained in zonal wavenumber two at all latitudes. This behaviour is strange since

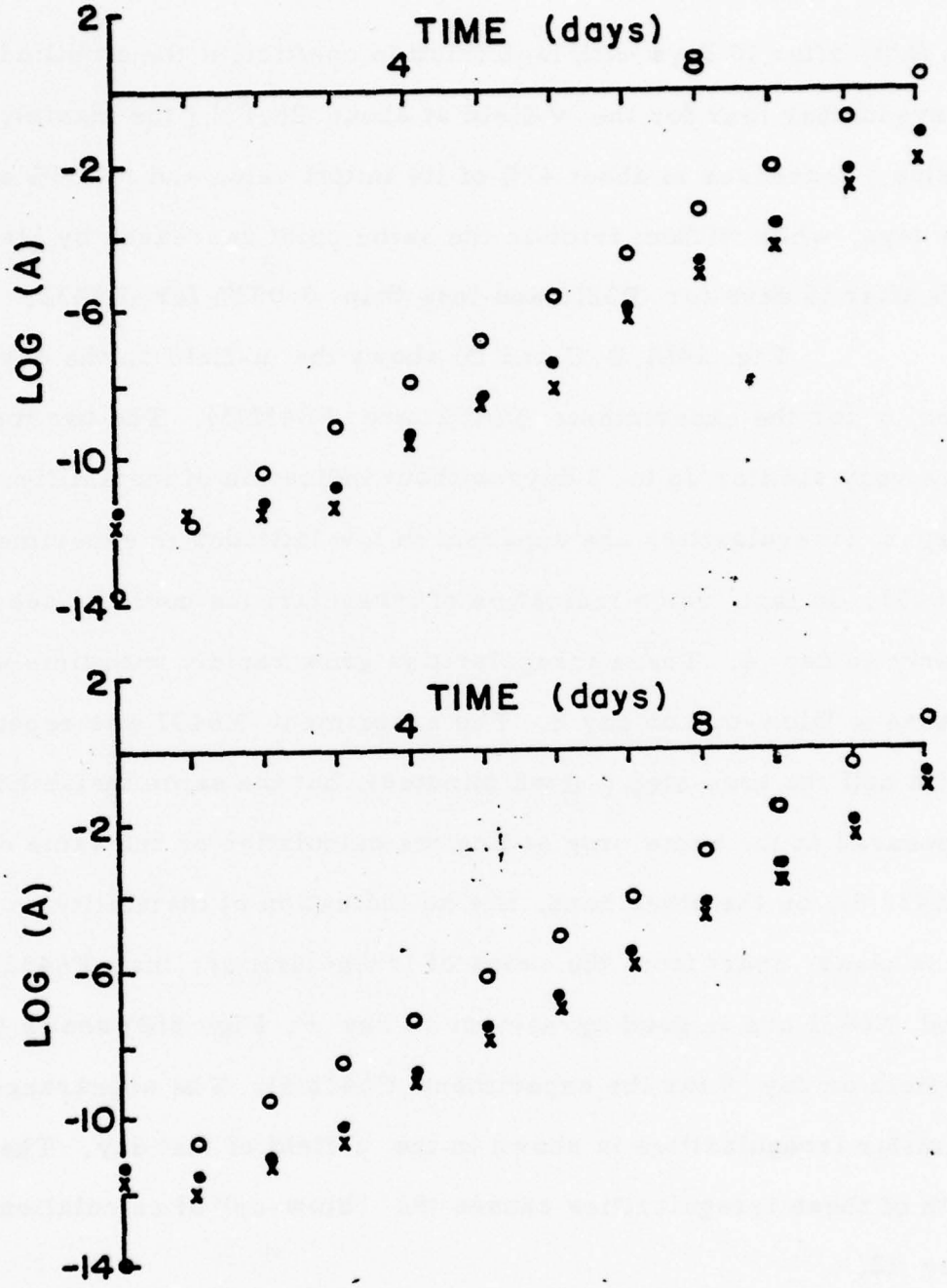

Fig. 15. The logarithmic distribution of the amplitude of wavenumber two as function of time at the latitudes 5.6°N (•), 39.4°N (x) and 84.4°N (o). The upper and lower curves are for the experiments N3216 and F3216(5) respectively.

neither the interaction of the primary wave (zonal wavenumber four) nor aliasing should develop zonal wavenumber two. Fig. 15 shows the distribution of the amplitude for zonal wavenumber two as function of time for the experiments N3216 and F3216(5). The irregularities grow with time and finally end the calculation on days 16 and 18 for N3216 and F3216(5) respectively. Note that the other experiments, including N6432 and F6432(5), shows practically zero magnitude for wavenumber two at all latitudes as far as the integration goes.

IV.4 Experiments with wavenumber 6

In section IV.3 a stable wave was studied and we saw that because of the reversable cascade of energy and enstrophy between large and small scale waves, the periodic filter with low resolution produced rather large differences in the evolution of the flow. In this section, we perform similar studies with initial conditions drawn from a Haurwitz wavenumber 6. As shown by many authors this wave breaks down in a few days forming cut off lows in middle latitudes (see for example Merilees (1974) and Kasahara (1977)). With this initial condition it is unwise to run the experiments with 3-grid-length filter for low resolution (II=32 and JJ=16), the initial disturbance has considerable energy in wavenumber 12. Merilees (1974) showed that due to the unstable nature of the flow and the resulting cascade of enstrophy to the shorter wavelengths, experiments with resolution up to 15 waves are not enough to predict the evaluation of this wave

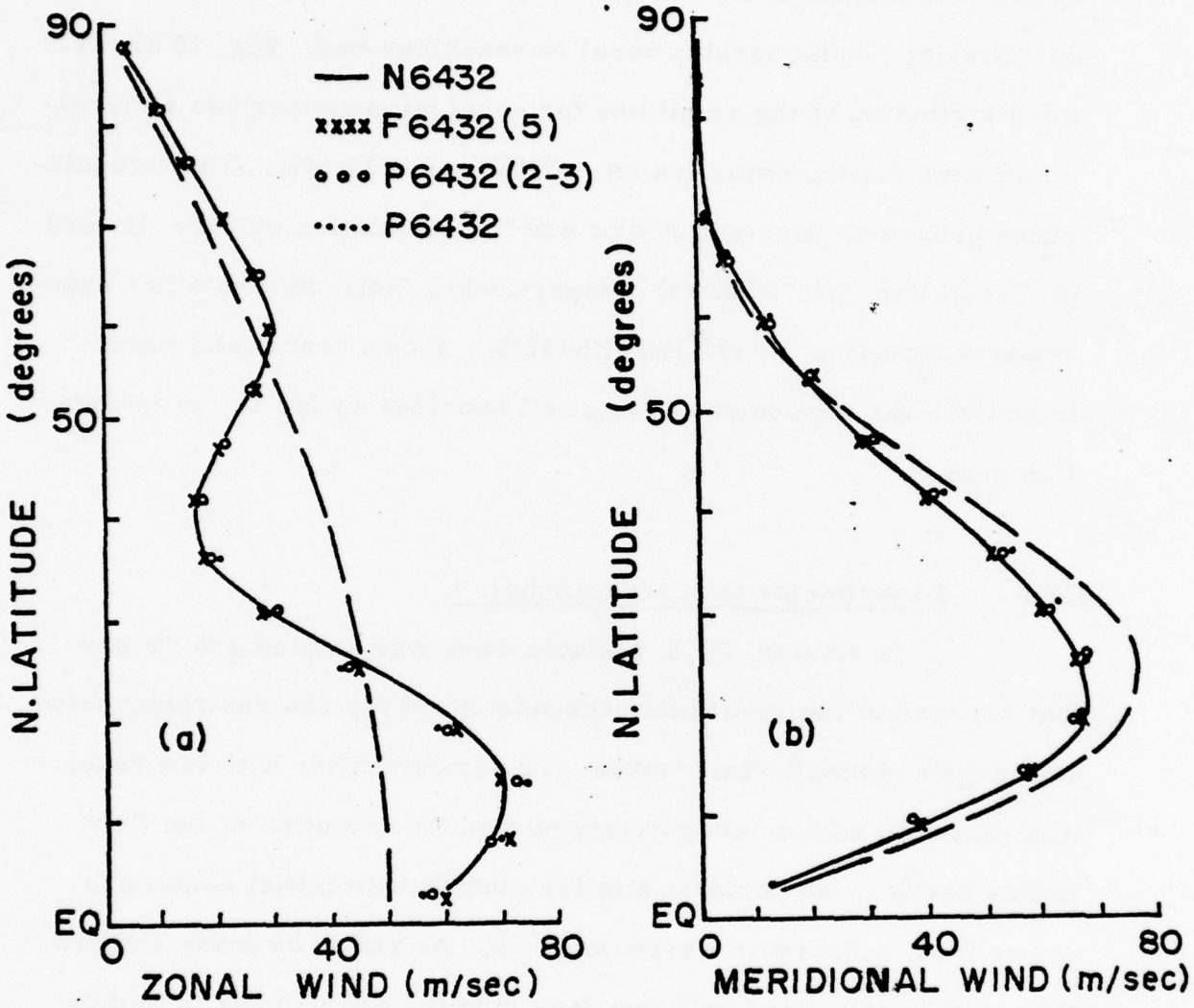

Fig. 16. (A): The zonal average of the u-field after 3 days as a function of latitude. (B): The amplitude of wavenumber 6 for the v-field after 3 days as a function of latitude. Thin dash line is the initial profile.

after 3 days. In this section the experiments N6432, F6432(5), P6432(2-3) and P6432 will be discussed. In addition a control run with filtering each time step and II=128 and JJ=64 was performed. The control run will be considered as the true solution. The time step used in these experiments is four minutes except for the control run where the time step is 5 minutes.

In each of the above five experiments the disturbance soon developed a north-west/south-east tilt which transported angular momentum out of the middle latitudes. The five models are in essential agreement up to 3 days with eastward phase progression of about 23.7° per day near the equator and 21.6° per day in high latitudes compared to 24.6° per day predicted by the non-divergent barotropic theory. Fig. 16(A and B) shows, on day 3, wavenumber 6 for the ν-field and the mean zonal flow for the experiments N6432, F6432(5), P6432(2-3) and P6432. After 3 days the differences between the above mentioned models become more noticeable. All the models indicate more rapid motion of the waves in low latitudes after 4 days. The main difference is in middle latitudes where experiments with Fourier filter show a stationary or weak westward motion of the waves at these latitudes after four days. The other experiments indicate weak eastward motion. This is shown on Fig.17(A and B) where we plot the distribution of the phase angle, of the primary wave for the ν-field, as function of time at the latitudes 30.9°N, 53.4°N and 70.3°N. As a result of the difference in phase speed with latitude between experiments with Fourier filter and the other experiments, the tilt of the

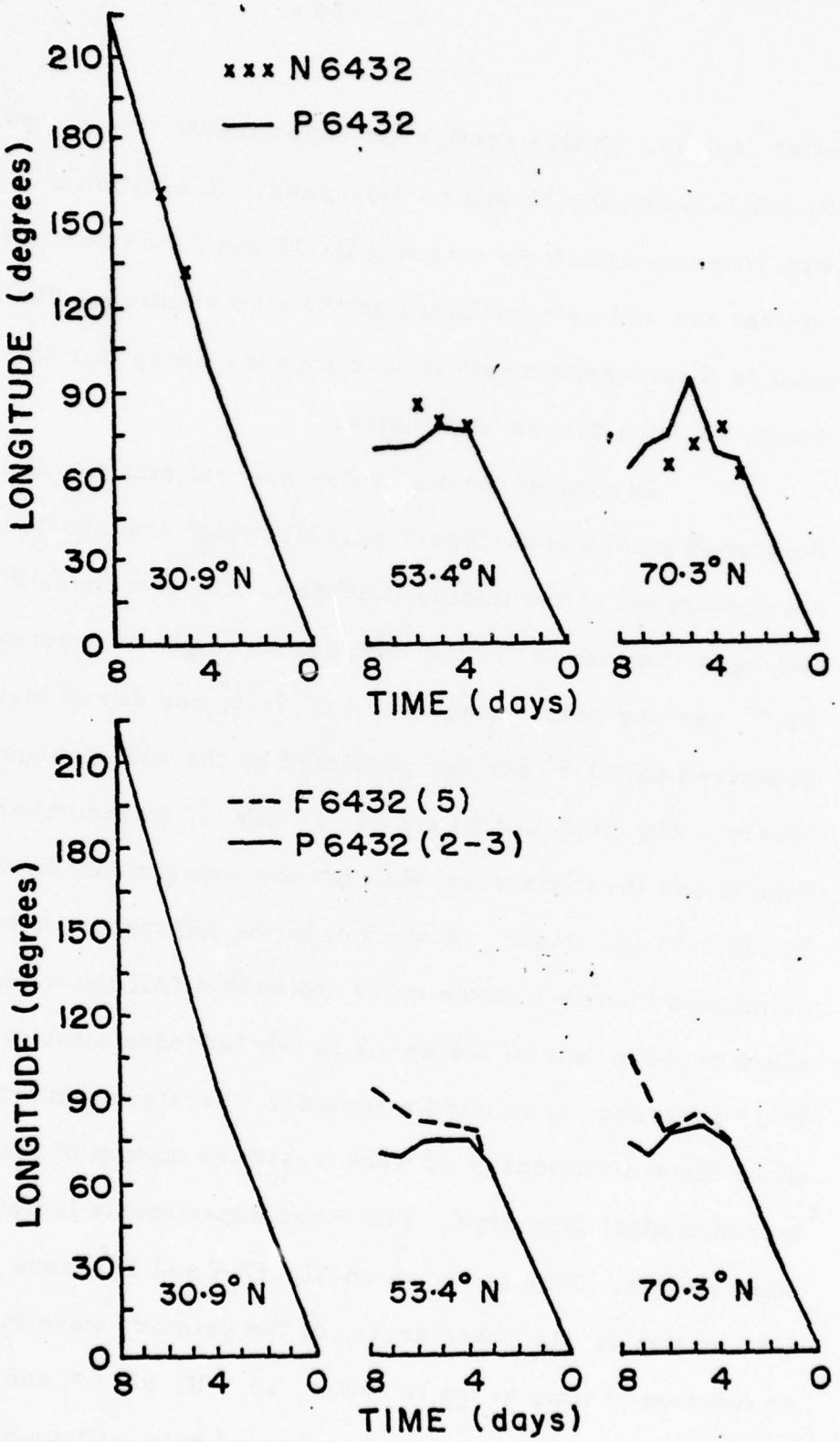

Fig. 17. The ridge position as function of time, for wavenumber 6, of the V-field at latitudes 30.9°N, 53.4°N and 70.3°N for the experiments N6432, P6432, F6432(5) and P6432(2-3).

the wave (which leads to the export of westerly momentum in middle latitudes) is steeper in P6432(2-3) and P6432 than F6432(5). This result in weaker easterlies for F6432(5) which can be seen on Fig.18(A). The latitudinal distribution of the mean zonal flow and the main wave for the $\sqrt{}$-field, on day 6 [Fig.18(A and B) and Fig.19(A and B)], indicate that the experiments with Fourier filter, on that day, are closer to the control run than the other experiments. N6432 shows clear irregularities on the mean zonal flow and the main disturbance of the $\sqrt{}$-field, Fig.18(A and B). N6432 shows an increase of kinetic energy of about 28% on day 6 and subsequently "blows-up", Fig.20. F6432(5) shows irregularities in low and high latitudes on day 8, Fig.21(A), and the calculation is ended after 9 days due to the accumulation of energy in high wavenumbers. At this time the kinetic energy has increased by about 53%, as shown in Fig.20. Fig.21 shows the h-fields, on day 8, for the experiments F6432(5), P6432(2-3), P6432 and the control run. Apart from the area of irregularities shown on the field of F6432(5), the comparison between the fields shows better result for the runs with the Fourier filter. For example, in middle latitudes F6432(5) shows open waves while, as expected from the results of others and also from our control run (Fig.21(D)), P6432(2-3) and P6432 give closed systems in middle latitudes.

It is clear from this section that the periodic filter does control the aliasing instability and at the same time gives reasonable evolution of the flow with time with little additional computing time. On the other hand for wavenumber 6 the friction term with coefficient

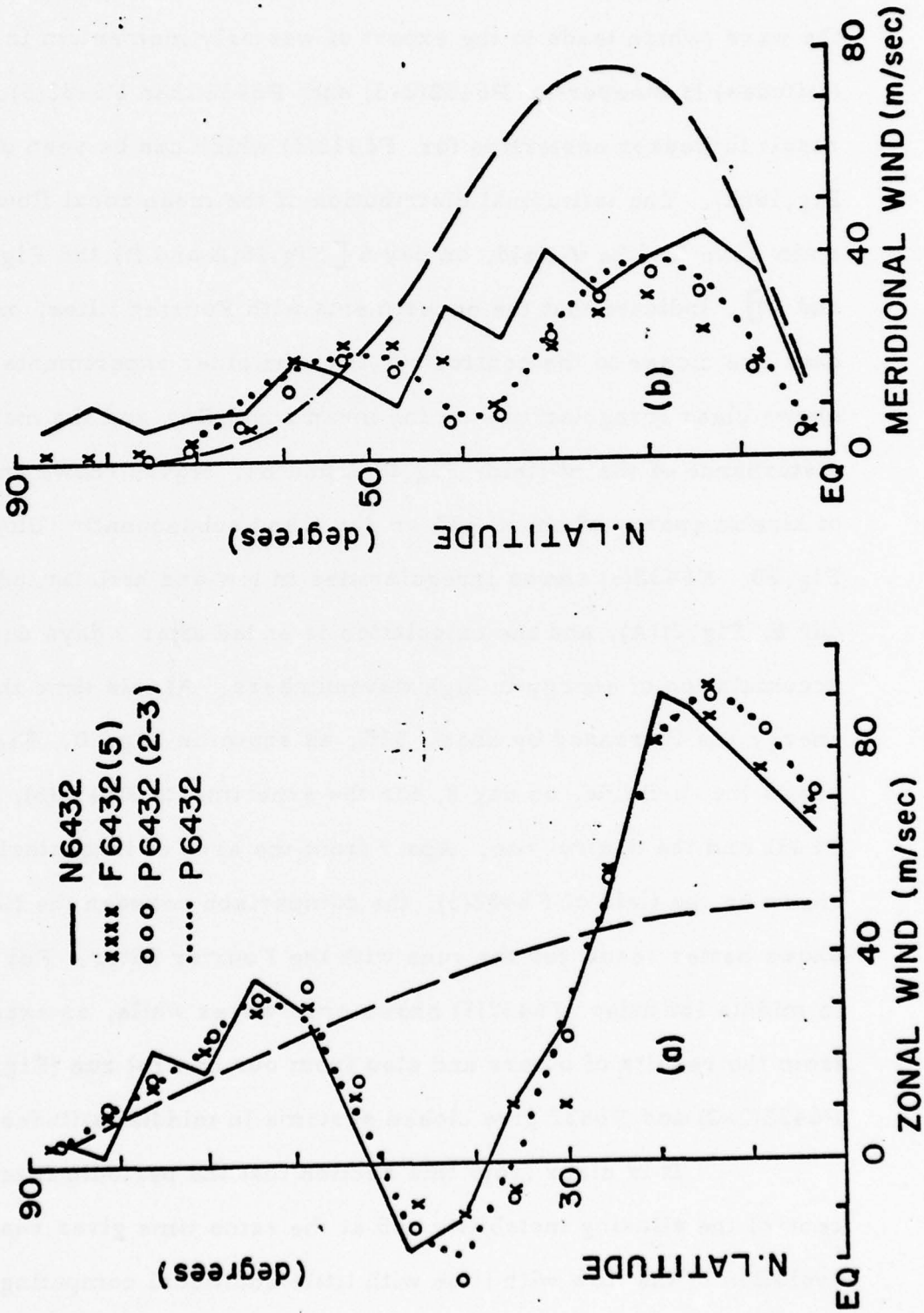

Fig. 18(A and B) - Same as Fig.16(A and B) except after 6 days.

of $10^5 m^2/sec$ is not enough to prevent the accumulation of energy in high wavenumbers and higher values of the friction coefficient will cause excessive smoothing.

From these experiments we cannot conclude that a non-linear viscous term would not do a better job, but certainly the results of Miyakoda et al (1971) indicate that such an approach is not too promising.

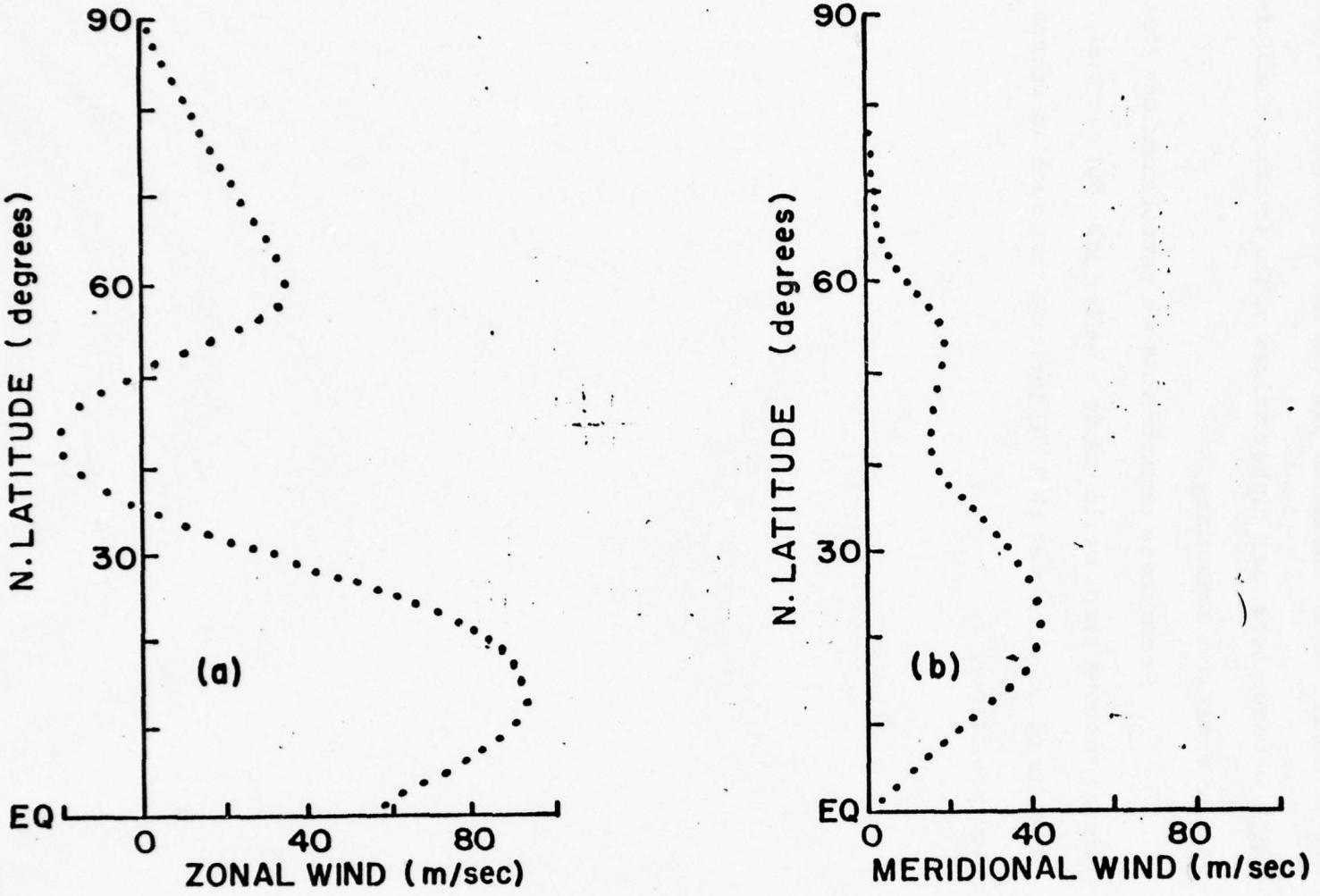

Fig. 19(A and B) - Same as Fig.16(A and B) except after 6 days for the control run.

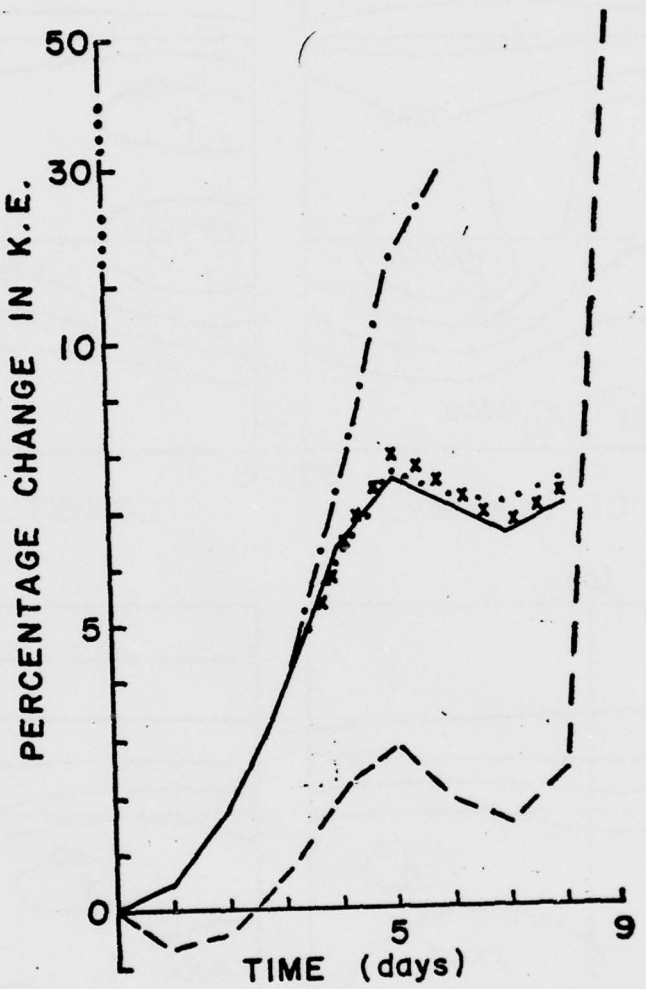

Fig. 20. The percentage change from initial time of the Kinetic Energy (K.E.) for the experiments N6432 (-----), F6432(5) (-----), P6432(2-3) (——), P6432 (xxxx) and the control run (••••), as function of time.

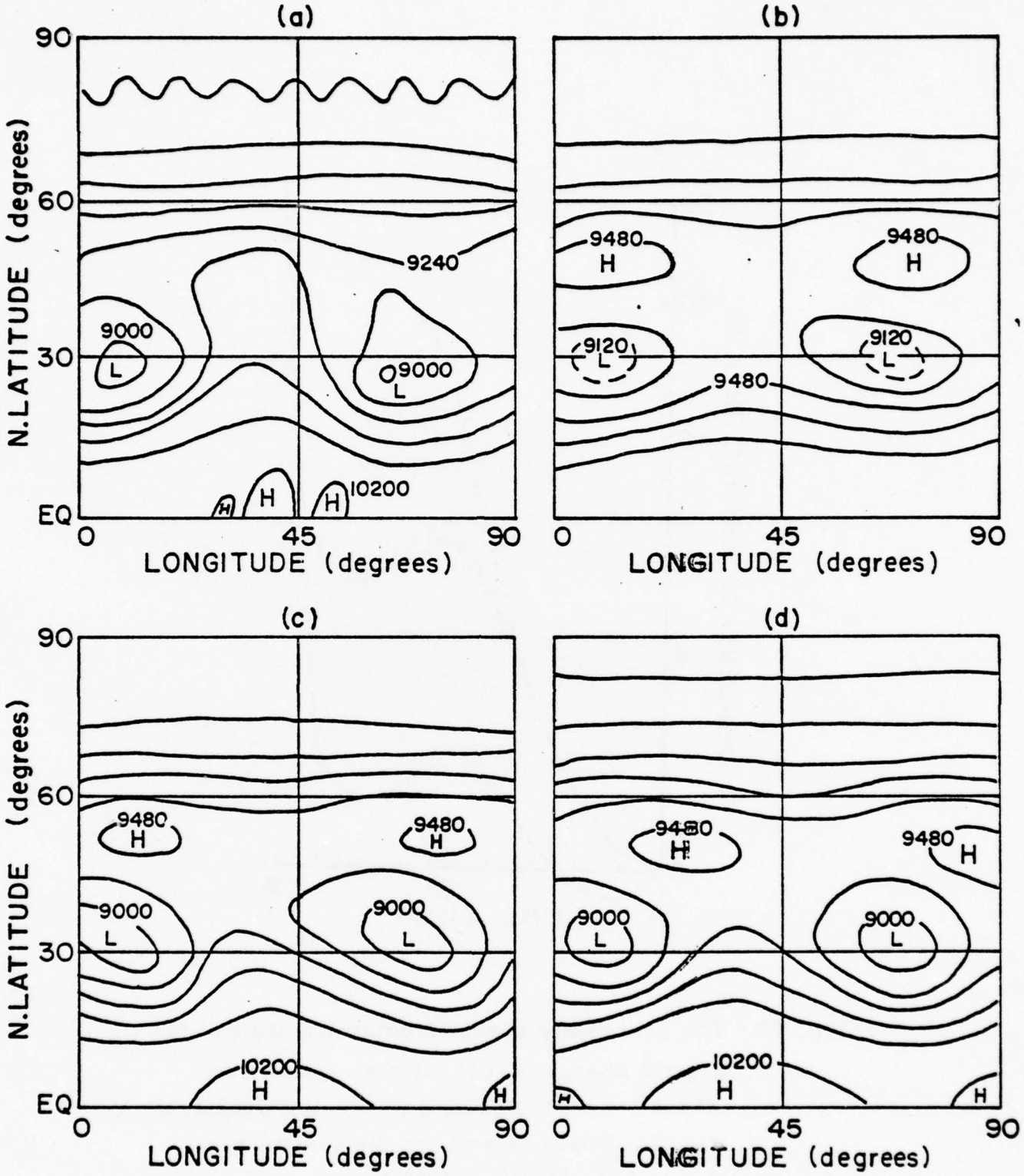

Fig. 21. The free surface height, after 8 days, for the models F6432(5), P6432(2-3), P6432 and the control run; A, B, C and D respectively. Contour interval is 240 meter.

CHAPTER V

SUMMARY AND CONCLUSIONS

One of the problems of long range forecast models is their need for some sort of smoothing to prevent the non-linear (aliasing) instability and to achieve reasonably smooth fields. Two methods are tried for a one level primitive global model. The use of a Fourier filter which eliminates the 3-gridlength waves and smaller from time to time, and the addition of a linear friction term, in the momentum equation, to dissipate the kinetic energy especially from small scale waves. The models are tested with two types of simple initial conditions, a stable wave where the fields tend to return back to their initial values and unstable wave where the fields break down within few days. Up to three or four days the models show no significant differences between the two approachs. In fact, even runs without any smoothing are in good agreement with them.

The 3-gridlength filter completely controls any instability up to the 20 day limit of our runs. It also requires little additional computer time. The time evolution of the flow is quite reasonable except if the filter interferes with an essential exchange of energy between the shorter and longer waves. In this case the filter can cause serious deviations from the true solution. In this case the solution to the error is to increase the resolution of the model.

On the other hand, a coefficient of viscosity equal 10^5 m^2/sec. fails to prevent the non-linear instability while a value of 10^6 m^2/sec

smoothed the fields too much. Further, the use of the friction term requires considerably more computer time as indicated in section II.8. Perhaps a nonlinear viscosity formulation would be more useful, but based on the work of Miyakoda et al (1971) this does not appear promising.

Somewhat surprisingly, the application of the 3-gridlength filter each time step gave the best overall results for both the stable and unstable wave. Such a procedure is however wasteful of resolution when the pseudospectral algorithm is used for the estimation of derivatives. Further, such a procedure would effectively convert the pseudospectral model into a spectral model with about 2/3 of the number of degrees of freedom. In that case it may well be more efficient to use a spectral model from the start.

While the results generally indicate that numerical filtering is better than a friction term, it is not obvious that the particular filter used is best. In fact, some less drastic form of numerical smoothing may be able to provide equally good long term numerical stability without strongly interfering with energy exchanges in a stable type flow.

Finally, it should be noted that these results have been obtained with very simple initial conditions. As such, they can only be indicative of sort of conclusion that would be obtained with initial conditions from real data.

BIBLIOGRAPHY

Bourke, W., 1972: An efficient, one-level, primitive equation spectral model. Mon. Wea. Rev., 100 , 683-689.

Chouinard, C., and A. J. Robert, 1972: Truncation errors in a filtered barotropic model. Proc. 9th Stanstead Seminar. Publ. in Meteorology No. 103, McGill Univ., 136pp.

Haurwitz, B., 1940: The motion of atmospheric disturbances on the spherical earth. J. marine Res., 3 , 254-267.

Hoskins, B. J., 1973: Stability of the Rossby-Haurwitz wave. Quart. J. Roy. Meteor. Soc., 99 , 723-745.

Jacques, G., 1976: Numerical experiments with a two-layer pseudospectral model of general circulation. M.Sc. Thesis, McGill University.

Kasahara, A., 1977: Numerical integration of the global barotropic primitive equations with Hough harmonic expansions. J. Atmos. Sci., 34 , 687-701.

McConnell, A. J., 1931: Application of tensor analysis. Dover Publ., Inc., New York.

Merilees, P. E., 1973: The pseudospectral approximation applied to the shallow water equations on a sphere. Atmosphere, 11 , 13-20.

———————, 1974: Numerical experiments with the pseudospectral method in spherical coordinates. Atmosphere, 12, 77-96.

———————, P. Ducharme and G. Jacques, 1976: Experiments with a polar filter and a one-dimensional semi-implicit algorithm. Atmosphere, 15 , 19-32.

Miyakoda, K., R. F. Strickler, C. J. Nappo, P. L. Baker and G. D. Hembree, 1971: The effect of horizontal grid resolution in an atmospheric circulation model. J. Atmos. Sci., 28 , 481-499.

Orszag, S. A., 1971: On the elimination of aliasing in finite-difference schemes by filtering high wavenumber components. J. Atmos. Sci., 28 , 1074-1078.

———————, 1972: Comparison of pseudospectral and spectral approximations. Studies in applied Mathematics, 51 , 253-259.

Phillips, N. A., 1959: Numerical integration of the primitive equations on the hemisphere. Mon. Rev., 87 , 333-345.

Appendix (I): Friction formula

Starting with the viscous force in the form

$$F_r = g^{st} \sigma_{rs,t} \tag{31}$$

where the stress tensor

$$\sigma_{rs} = \nu \left(V_{r,s} + V_{s,r} \right) \tag{32}$$

For surface spherical polar coordinates the distance ds in two dimension is defined as

$$(ds)^2 = a^2 (d\theta)^2 + a^2 \sin^2\theta \ (d\lambda)^2,$$

where λ longitude and θ colatitude.

Or, $(ds)^2 = a^2 (dx_1)^2 + a^2 \sin^2 x_1 \ (dx_2)^2$,

where

$$g_{11} = a^2 \qquad \text{and} \qquad g_{22} = a^2 \sin^2 x_1,$$

and

$$g^{11} = \frac{1}{a^2} \qquad \text{and} \qquad g^{22} = \frac{1}{a^2 \sin^2 x_1}.$$

Now

$$V_{r,s} = \frac{\partial V_r}{\partial x^s} - \left\{ \begin{matrix} m \\ rs \end{matrix} \right\} V_m = \frac{\partial V_r}{\partial x^s} - \left\{ \begin{matrix} 1 \\ rs \end{matrix} \right\} V_1 - \left\{ \begin{matrix} 2 \\ rs \end{matrix} \right\} V_2, \tag{33}$$

where $\left\{ \begin{matrix} m \\ rs \end{matrix} \right\}$ is Christoffel symbol of the second kind defined as

$$\left\{ \begin{matrix} m \\ rs \end{matrix} \right\} = g^{rp} [mn, p].$$

$[mn, p]$ is Christoffel symbol of the first kind defined as

$$[mn, p] = \frac{1}{2} \left(\frac{\partial g_{np}}{\partial x^m} + \frac{\partial g_{pm}}{\partial x^n} - \frac{\partial g_{mn}}{\partial x^p} \right).$$

It is easy to prove that

$$[11,1] = [11,2] = [12,1] = [21,1] = [22,2] = 0 ,$$

and

$$[12,2] = a^2 \sin x_1 \cos x_1 ,$$

$$[21,2] = a^2 \sin x_1 \cos x_1 ,$$

$$[22,1] = -a^2 \sin x_1 \cos x_1 .$$

So

$$\begin{Bmatrix} 1 \\ 2\,2 \end{Bmatrix} = -\sin x_1 \cos x_1 \qquad \text{and} \qquad \begin{Bmatrix} 2 \\ 2\,1 \end{Bmatrix} = \cot x_1 = \begin{Bmatrix} 2 \\ 1\,2 \end{Bmatrix} .$$

From (33)

$$V_{1,1} = \frac{\partial V_1}{\partial x^1} ,$$

$$V_{2,1} = \frac{\partial V_2}{\partial x^1} - \cot x_1 \, V_2 ,$$

$$V_{1,2} = \frac{\partial V_1}{\partial x^2} - \cot x_1 \, V_2 ,$$

and $$V_{2,2} = \frac{\partial V_2}{\partial x^2} + \sin x_1 \cos x_1 \, V_1 ,$$

and from (32)

$$\sigma_{11} = \nu (V_{1,1} + V_{1,1}) = 2\nu \frac{\partial V_1}{\partial x^1}$$

$$\sigma_{22} = \nu (V_{2,2} + V_{2,2}) = 2\nu (\frac{\partial V_2}{\partial x^2} + \sin x_1 \cos x_1 \, V_1),$$

and $$\sigma_{12} = \sigma_{21} = \nu (\frac{\partial V_2}{\partial x^1} + \frac{\partial V_1}{\partial x^2} - 2\cot x_1 \, V_2).$$

Now in terms of physical components

$$V_\theta = V^1/h_1 = g^{11} V_1 / h_1 = V_1 / a ,$$

$$V_\lambda = V^2/h_2 = g^{22} V_2 / h_2 = V_2 / (a \sin\theta).$$

Or

$$V_1 = a \, V_\theta \qquad \text{and} \qquad V_2 = a \sin\theta \, V_\lambda ,$$

further

$$\sigma_{\theta\theta} = h_1^2 \sigma_{11} = \sigma_{11} / a^2 = \frac{2\nu}{a^2} \frac{\partial}{\partial\theta} (a V_\theta) = \frac{2\nu}{a} \frac{\partial V_\theta}{\partial\theta} ,$$

$$\sigma_{\lambda\lambda} = h_2^2 \sigma_{22} = \frac{2\nu}{a^2 \sin\theta} \left[\frac{\partial (a \sin\theta \, V_\lambda)}{\partial\lambda} + \sin\theta \cos\theta \, a V_\lambda \right] .$$

Or

$$\sigma_{\lambda\lambda} = \frac{2\nu}{a \sin\theta}\left[\frac{\partial V_\lambda}{\partial \lambda} + \cos\theta\, V_\theta\right],$$

and

$$\sigma_{\theta\lambda} = \sigma_{\lambda\theta} = \frac{\nu}{a \sin\theta}\left[\sin\theta \frac{\partial V_\lambda}{\partial \theta} + \frac{\partial V_\theta}{\partial \lambda} - \cos\theta\, V_\lambda\right].$$

As $F_r = g^{st}\sigma_{rs,t}$ and $\sigma_{rs,t} = \frac{\partial \sigma_{rs}}{\partial x^t} - \left\{ {m \atop st} \right\}\sigma_{rm} - \left\{ {m \atop rt} \right\}\sigma_{ms}$,

$$\therefore \quad F_r = g^{11}\sigma_{r1,1} + g^{22}\sigma_{r2,2} = \frac{1}{a^2}\sigma_{r1,1} + \frac{1}{a^2\sin^2\theta}\sigma_{r2,2}, \qquad (34)$$

where

$$\sigma_{r1,1} = \frac{\partial \sigma_{r1}}{\partial x^1} - \left\{ {m \atop 11} \right\}\sigma_{rm} - \left\{ {m \atop r1} \right\}\sigma_{m1},$$

$$= \frac{\partial \sigma_{r1}}{\partial x^1} - \left\{ {1 \atop r1} \right\}\sigma_{11} - \left\{ {2 \atop r1} \right\}\sigma_{21}.$$

So

$$\sigma_{11,1} = \frac{\partial \sigma_{11}}{\partial \theta} \quad \text{and} \quad \sigma_{21,1} = \frac{\partial \sigma_{21}}{\partial \theta} - \cot\theta\,\sigma_{21}.$$

Also

$$\sigma_{r2,2} = \frac{\partial \sigma_{12}}{\partial x^2} - \left\{ {m \atop 22} \right\}\sigma_{rm} - \left\{ {m \atop r2} \right\}\sigma_{m2},$$

$$= \frac{\partial \sigma_{12}}{\partial \lambda} + \sin x_1 \cos x_1\, \sigma_{r1} - \left\{ {1 \atop r2} \right\}\sigma_{12} - \left\{ {2 \atop r2} \right\}\sigma_{22}.$$

$$\therefore \sigma_{12,2} = \frac{\partial \sigma_{12}}{\partial \lambda} + \sin\theta\cos\theta\,\sigma_{11} - \cot\theta\,\sigma_{22}$$

and

$$\sigma_{22,2} = \frac{\partial \sigma_{22}}{\partial \lambda} + 2\sin\theta\cos\theta\,\sigma_{12}.$$

So from (34)

$$F_1 = \frac{1}{a^2}\sigma_{11,1} + \frac{1}{a^2\sin^2\theta}\sigma_{12,2}$$

$$= \frac{\partial \sigma_{\theta\theta}}{\partial \theta} + \frac{1}{\sin\theta}\frac{\partial \sigma_{\theta\lambda}}{\partial \lambda} + \cot\theta\,\sigma_{\theta\theta} - \cot\theta\,\sigma_{\lambda\lambda},$$

or

$$F_6 = \frac{1}{a}\left\{\frac{\partial \sigma_{\theta\theta}}{\partial \theta} + \frac{1}{\sin\theta}\frac{\partial \sigma_{\theta\lambda}}{\partial \lambda} + \cot\theta\,\sigma_{\theta\theta} - \cot\theta\,\sigma_{\lambda\lambda}\right\}.$$

Similarly we can prove that

$$F_\lambda = \frac{1}{a}\left\{ \frac{\partial \sigma_{\theta\lambda}}{\partial \theta} + \frac{1}{\sin\theta}\frac{\partial \sigma_{\lambda\lambda}}{\partial \lambda} + 2\cot\theta\,\sigma_{\theta\lambda} \right\}.$$

To get the equations in terms of φ (latitude) and λ (longitude) and to replace V_θ and V_λ by $-v$ and u as meteorologist generally do, we use the following relations

$$\varphi = \pi/2 - \theta \quad , \quad V_\theta = -v \quad \text{and} \quad V_\lambda = u.$$

Then it is possible to prove that

$$F_\varphi = \nu/a^2\left\{ 2\frac{\partial^2 v}{\partial \varphi^2} + \frac{1}{\cos\varphi}\frac{\partial^2 u}{\partial \varphi \partial \lambda} + \frac{1}{\cos^2\varphi}\frac{\partial^2 v}{\partial \lambda^2} + \frac{3\sin\varphi}{\cos^2\varphi}\frac{\partial u}{\partial \lambda} - 2\tan\varphi\frac{\partial v}{\partial \varphi} - \frac{2\sin^2\varphi}{\cos^2\varphi}v \right\},$$

and

$$F_\lambda = \nu/a^2\left\{ \frac{\partial^2 u}{\partial \varphi^2} + \frac{1}{\cos\varphi}\frac{\partial^2 v}{\partial \varphi \partial \lambda} - \frac{3\sin\varphi}{\cos^2\varphi}\frac{\partial v}{\partial \lambda} - \tan\varphi\frac{\partial u}{\partial \varphi} - \left(2\tan^2\varphi - \frac{1}{\cos^2\varphi}\right)u + \frac{2}{\cos^2\varphi}\frac{\partial^2 u}{\partial \lambda^2} \right\}.$$

Appendix (II): CFL criterion

In order to obtain guidelines for the choise of time step we treat the numerical stability problem in Cartesian rather than spherical coordinates. This approach was taken by Jacques(1976) with useful results. Here we include a friction term. Consider in Cartesian coordinates the following equations

$$\frac{\partial u}{\partial t} = -\frac{\partial \Phi}{\partial x} + \nu\left(\frac{\partial^2 u}{\partial x^2} + \frac{\partial^2 u}{\partial y^2}\right),$$

$$\frac{\partial v}{\partial t} = -\frac{\partial \Phi}{\partial y} + \nu\left(\frac{\partial^2 v}{\partial x^2} + \frac{\partial^2 v}{\partial y^2}\right),$$

and $$\frac{\partial \Phi}{\partial t} = -\Phi\left(\frac{\partial u}{\partial x} + \frac{\partial v}{\partial y}\right),$$

where $\Phi = g\overline{H}$ is a constant.

Using Fourier series, let us express all the dependent variables in the form

$$A = \sum_k \sum_l A_0 e^{i(kx+ly)},$$

A is function of time, k is the east-west wavenumber and l is the north-south wavenumber. Using a leapfrog time scheme and remembering that the space derivatives are exact, the finite differences analogues to the above equation, for a particular mode k and l, can be written as

$$u_0^{t+\Delta t} - u_0^{t-\Delta t} = -2\Delta t\left[iK\Phi_0^t + \nu u_0^{t-\Delta t}(K^2+l^2)\right],$$

$$v_0^{t+\Delta t} - v_0^{t-\Delta t} = -2\Delta t\left[il\Phi_0^t + \nu v_0^{t-\Delta t}(K^2+l^2)\right],$$

$$\Phi_0^{t+\Delta t} - \Phi_0^{t-\Delta t} = -2i\Delta t\,\Phi\left[K u_0^t + l v_0^t\right],$$

where we have used the standard technique of calculating the friction term at time $t - \Delta t$.

Assuming solutions of the form

$$\begin{pmatrix} u_0 \\ v_0 \\ \phi_0 \end{pmatrix} = \begin{pmatrix} u^* \\ v^* \\ \phi^* \end{pmatrix} e^{i\omega t}, \tag{35}$$

where u^*, v^*, and ϕ^* are constants, we find that

$$u^*(\lambda - \bar{\lambda}^{-1}) + 2\nu\,\Delta t\,\lambda^{-1}(k^2+l^2)u^* + 2i\,\Delta t\,k\,\Phi^* = 0,$$

$$v^*(\lambda - \bar{\lambda}^{-1}) + 2\nu\,\Delta t\,\lambda^{-1}(k^2+l^2)v^* + 2i\,\Delta t\,l\,\Phi^* = 0,$$

$$\Phi^*(\lambda - \bar{\lambda}^{-1}) + 2i\,\Delta t\,\Phi k u^* + 2i\,\Delta t\,\Phi l v^* = 0,$$

where $\lambda = e^{i\omega\Delta t}$.

The condition for a non-trival solution is that the determinant of the algebraic system vanish, i.e.

$$\begin{vmatrix} (\lambda-\bar{\lambda}^{-1}) + 2\nu\,\Delta t\,\lambda^{-1}(k^2+l^2) & 0 & 2i\Delta t k \\ 0 & (\lambda-\bar{\lambda}^{-1}) + 2\nu\,\Delta t\,\bar{\lambda}^{-1}(k^2+l^2) & 2i\Delta t l \\ 2i\,\Delta t\,\Phi k & 2i\Delta t\,\Phi l & (\lambda-\bar{\lambda}^{-1}) \end{vmatrix} = 0.$$

If we denote $A = (\lambda - \bar{\lambda}^{-1}) + 2\nu\,\Delta t\,\bar{\lambda}^{-1}(k^2+l^2)$,

then expansion of the determinant yields the condition

$$A\left\{(\lambda - \bar{\lambda}^{-1})A + 4(\Delta t)^2\,\Phi\,(k^2+l^2)\right\} = 0.$$

In order for the calculation to be stable we must have all possible

values of λ to be such that $|\lambda| \leq 1$.

Case 1.

The first case we consider is when the first factor in the above condition is zero, i.e.

$$(\lambda - \bar{\lambda}^{-1}) + 2\nu\,\Delta t\,(k^2+\ell^2)\lambda^{-1} = 0,$$

or

$$\lambda^2 = 1 - 2\nu\,\Delta t\,(k^2+\ell^2).$$

Then to insure stability we require that

$$-1 \leq 1 - 2\nu\,\Delta t\,(k^2+\ell^2) \leq 1.$$

The r.h.s. is always satisfied. The l.h.s. gives a condition for stability

$$\Delta t \leq 1/\nu\,(k^2+\ell^2).$$

Without friction these modes are neutral, with friction we expect the modes to be exponentially damped. Note however that if

$$1/\nu(k^2+\ell^2) \geq \Delta t \geq 1/2\nu\,(k^2+\ell^2),$$

then $\lambda^2 < 0$ and the solution is not physically realistic since there will be a sign change each second time step. Thus a reasonable condition to impose is

$$\Delta t \leq 1/2\nu\,(k^2+\ell^2).$$

Case 2.

When the second factor is zero we have

$$(\lambda - \bar{\lambda}^{-1})^2 + 2\nu\,\Delta t\,(k^2+\ell^2)\bar{\lambda}^{-1}(\lambda - \bar{\lambda}^{-1}) + 4(\Delta t)^2\Phi\,(k^2+\ell^2) = 0,$$

or $$(\lambda^2 - 1)^2 + 2\nu\,\Delta t\,(k^2+\ell^2)\,(\lambda^2 - 1) + 4\,(\Delta t)^2\Phi\,(k^2+\ell^2)\lambda^2 = 0.$$

Putting

$$a = \nu \Delta t \, (k^2 + \ell^2) \qquad \text{and} \qquad b = 2(\Delta t)^2 \Phi \, (k^2 + \ell^2),$$

the above equation can be written as

$$(\lambda^2 - 1)^2 + 2a (\lambda^2 - 1) + 2b (\lambda^2 - 1) + 2b = 0 ,$$

or

$$X^2 + 2 (a + b) X + 2b = 0 ,$$

where $X = \lambda^2 - 1$.

So $$X = - (a + b) \pm \sqrt{(a + b)^2 - 2b} ,$$

or

$$\lambda^2 = 1 - (a + b) \pm \left[(a + b) - 2b \right]^{1/2} .$$

Suppose that

$$(a + b)^2 - 2b < 0 ,$$

then the stability condition $|\lambda^2| \leq 1$ implies that

$$\left[(1 - a - b)^2 - \{ (a + b)^2 - 2b \} \right]^{1/2} \leq 1 ,$$

or

$$(1 - 2a)^{1/2} \leq 1 .$$

By definition $a \geq 0$ and since we have choosen $a \leq 1/2$, from the study of the first factor, we find that this condition is always satisfied. But if

$$(a + b)^2 - 2b \geq 0 ,$$

then $|\lambda^2| \leq 1$ implies that

$$-1 \leq 1 - (a + b) \pm \left[(a + b)^2 - 2b \right]^{1/2} \leq 1 .$$

The r.h.s. is always satisfied since

$$\left| \left[(a + b)^2 - 2b \right]^{1/2} \right| \leq | a + b | .$$

The possible problem root is the lower sign on the radical, since it

will contribute to decreasing the middle expression. It is therefore necessary and sufficient that

$$1 - (a+b) - \left[(a+b)^2 - 2b\right]^{\frac{1}{2}} \geq -1 ,$$

or

$$(a+b) + \left[(a+b)^2 - 2b\right]^{\frac{1}{2}} \leq 2 .$$

It follows that

$$\left[(a+b)^2 - 2b\right]^{\frac{1}{2}} \leq 2 - (a+b) .$$

Now if $(a+b) > 2$, then the inequality can never be satisfied, therefore

$$2 - (a+b) \text{ must be } \geq 0 .$$

Then it is possible to square the previous inequality, which gives

$$2 \geq 2a + b ,$$

or

$$1 \geq \nu(\Delta t)(k^2 + l^2) + (\Delta t)^2 \Phi (k^2 + l^2) .$$

Without friction this condition reads

$$\Delta t \leq 1/(k^2 + l^2)^{\frac{1}{2}} C , \qquad (36)$$

where $C = (g\bar{H})^{\frac{1}{2}}$ is the speed of gravity waves.

In our experiments $\bar{H} = 8$ km and the largest value used for ν, the kinematic viscosity, is 10^6 m^2/sec. Also the smallest value used for Δt, in our experiments, is one minute. This means that in our experiments $\Delta t \Phi$ is greater or of the same order as ν. So with fully explicit scheme we can say, in our experiments, that the friction do not have significant effect on the CFL criterion which can be considered (36).

Let us now integrate the same system of equations using the one dimensional semi-implicit scheme discussed in II.4. Using

a leapfrog time scheme, then for a particular mode k and ℓ we get

$$u_o^{t+\Delta t} - u_o^{t-\Delta t} = -2\,\Delta t\left[ik\frac{\Phi_o^{t+\Delta t} + \Phi_o^{t-\Delta t}}{2} + \nu\left(k^2 u_o^{t-\Delta t} + \ell^2 u_o^{t-\Delta t}\right)\right],$$

$$v_o^{t+\Delta t} - v_o^{t-\Delta t} = -2\,\Delta t\left[i\ell\,\Phi_o^{t} + \nu\, v_o^{t-\Delta t}\left(k^2 + \ell^2\right)\right],$$

$$\Phi_o^{t+\Delta t} - \Phi_o^{t-\Delta t} = -2i\,\Delta t\,\Phi\left[k\,\frac{u_o^{t+\Delta t} + u_o^{t-\Delta t}}{2} + \ell\, v_o^{t}\right].$$

Assuming solution in the form (35), the equations become, with

$$\lambda = e^{i\omega\Delta t},$$

$$u^*\left(\lambda - \lambda^{-1}\right) + i\,\Delta t\,k\,\Phi^*\left(\lambda + \lambda^{-1}\right) + 2\nu\,\Delta t\,\lambda^{-1}\left(k^2+\ell^2\right)u^* = 0,$$

$$v^*\left(\lambda - \lambda^{-1}\right) + 2i\,\Delta t\,\ell\,\Phi^* + 2\nu\,\Delta t\,\lambda^{-1}\left(k^2+\ell^2\right)v^* = 0,$$

$$\Phi^*\left(\lambda - \lambda^{-1}\right) + i\,\Delta t\,\Phi\,k\left(\lambda + \lambda^{-1}\right)u^* + 2i\,\Delta t\,\Phi\,\ell\,v^* = 0.$$

u^*, v^* and Φ^* have non-trivial solution if

$$\begin{vmatrix} \left(\lambda - \lambda^{-1}\right) + 2\nu\,\Delta t\,\lambda^{-1}\left(k^2+\ell^2\right) & 0 & i\,\Delta t\,k\left(\lambda + \lambda^{-1}\right) \\ 0 & \left(\lambda - \lambda^{-1}\right) + 2\nu\,\Delta t\,\lambda^{-1}\left(k^2+\ell^2\right) & 2i\,\Delta t\,\ell \\ i\,\Phi\,\Delta t\,k\left(\lambda + \lambda^{-1}\right) & 2i\,\Delta t\,\Phi\,\ell & \left(\lambda - \lambda^{-1}\right) \end{vmatrix} = 0.$$

With $A = \left(\lambda - \lambda^{-1}\right) + 2\nu\,\Delta t\,\lambda^{-1}\left(k^2+\ell^2\right)$, we get

$$A\left[\left(\lambda - \lambda^{-1}\right)A + 4\left(\Delta t\right)^2\Phi\,\ell^2 + \left(\Delta t\right)^2 k^2\,\Phi\left(\lambda + \lambda^{-1}\right)\right] = 0.$$

Which gives

$$A = 0,$$

with the condition of stability, as discussed before, namely

$$\Delta t \leq 1 / 2\nu\left(k^2+\ell^2\right).$$

The other solution gives

$$(\lambda - \bar{\lambda}^{-1})^2 + 2\nu(\Delta t)\bar{\lambda}^{-1}(\lambda - \bar{\lambda}^{-1})(k^2 + \ell^2) + 4(\Delta t)^2 \Phi \ell^2 + \\ + (\Delta t)^2 k^2 \Phi (\lambda + \bar{\lambda}^{-1})^2 = 0,$$

or

$$(\lambda^2 - 1)^2 + 2\nu(\Delta t)(k^2 + \ell^2)(\lambda^2 - 1) + (\Delta t)^2 k^2 \Phi (\lambda^2 + 1)^2 + \\ + 4(\Delta t)^2 \Phi \ell^2 \lambda^2 = 0.$$

Putting

$$a = \nu \Delta t (k^2 + \ell^2), \qquad b = (\Delta t)^2 k^2 \Phi \quad \text{and} \quad c = 2(\Delta t)^2 \Phi \ell^2,$$

the previous equation reads

$$X^2 (1 + b) + 2X(a + 2b + c) + 2(2b + c) = 0,$$

where

$$X = \lambda^2 - 1.$$

$$\therefore \quad X = \left\{ -(a + 2b + c) \pm \left[(a + 2b + c)^2 - 2(1+b)(2b+c) \right]^{1/2} \right\} / (1+b)$$

or

$$\lambda^2 = 1 + \frac{1}{(1+b)} \left\{ -(a+2b+c) \pm \left[(a+2b+c)^2 - 2(1+b)(2b+c) \right]^{1/2} \right\}$$

Following the same procedure as before, we get as a condition for stability

$$1 \geq \nu(\Delta t)(k^2 + \ell^2) + (\Delta t)^2 \Phi \ell .$$

The condition without friction is

$$\Delta t \leq 1 / \ell c .$$

Appendix (III): The relation between the momentum transport and the tilt of the v-field

In the northern hemisphere a north (south) transport of westerly momentum is associated with north-west/south-east (north-east/south-west) tilt of the v-field. This relationship between the tilt of the v-component of wind and the direction of momentum transport is strictly valid only in the case of geostrophic winds. Here we perform a sample calculation of the actual momentum transport to indicate that this relationship is valid for the numerical experiments described.

The momentum transport across a given latitude circle is proportional to

$$\frac{1}{2\pi} \int_0^{2\pi} u' v' \, d\lambda ,$$

where u' and v' are the deviations of the velocity components from the zonal average. In the sample calculation, by far the dominant component is wavenumber four. Therefore we can write

$$u' = A \cos (4\lambda - \varphi_u) ,$$

$$v' = B \cos (4\lambda - \varphi_v) ,$$

where A and B are the amplitudes for u' and v'. φ_u and φ_v are the phase angles.

It follows that the momentum transport can be written as

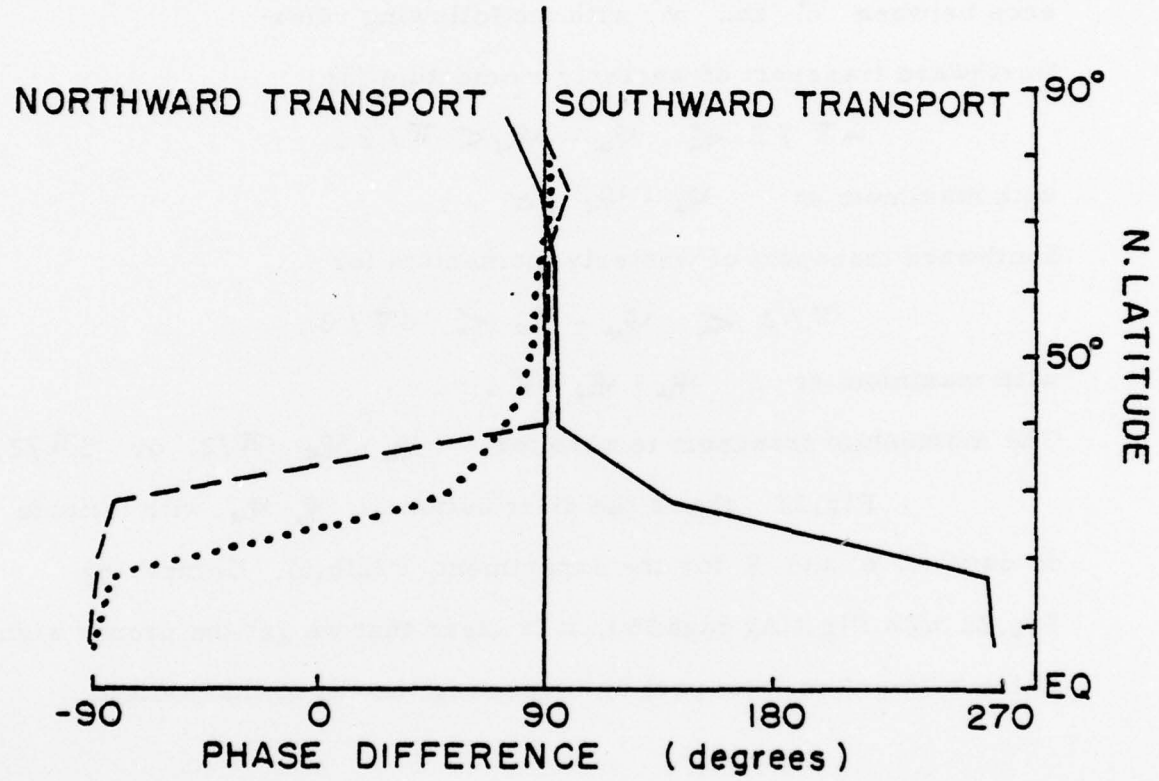

Fig. 22. The latitudinal distribution of the difference between the phase angles, for wavenumber 4, of the u and v fields for the experiment F3216(5). After 3 days (solid line), 6 days (dash line) and 9 days (dot line).

$$\frac{1}{2\pi}\int_0^{2\pi} u'v'\,d\lambda = \frac{1}{2\pi}\int_0^{2\pi} AB\,\cos(4\lambda - \varphi_u)\cos(4\lambda - \varphi_v)\,d\lambda$$

$$= \frac{AB}{2}\cos(\varphi_u - \varphi_v)\,.$$

The previous equation shows that the direction of the momentum transport across a latitude circle is determined by the phase difference between u' and v' with the following rules:

Northward transport of westerly momentum for

$$-\pi/2 < \varphi_u - \varphi_v < \pi/2\,,$$

with maximum at $\varphi_u - \varphi_v = 0$.

Southward transport of westerly momentum for

$$\pi/2 < \varphi_u - \varphi_v < 3\pi/2\,,$$

with maximum at $\varphi_u - \varphi_v = \pi$.

The momentum transport is zero for, $\varphi_u - \varphi_v = \pi/2$ or $3\pi/2$.

Fig.22 shows the distribution of $\varphi_u - \varphi_v$ with latitude on days 3, 6 and 9 for the experiment F3216(5). Comparing Fig.22 with Fig.3(A)(page 33), it is clear that we get the proper sign of the momentum transport by inspecting the tilt of the v-field.